1   **Immunotherapy-related cognitive impairment after CAR T cell therapy in mice**

2   Anna C. Geraghty[1,*], Lehi Acosta-Alvarez[1,*], Maria Rotiroti[2], Selena Dutton[1], Michael R. O'Dea[3],

3   Pamelyn J. Woo[1], Haojun Xu[1], Kiarash Shamardani[1], Rebecca Mancusi[1], Lijun Ni[1], Sara B.

4   Mulinyawe[1], Won Ju Kim[2], Shane A. Liddelow[3-6], Robbie G. Majzner[2,7], Michelle Monje[1,2,7,8]

5

6   1 Department of Neurology and Neurosciences, Stanford School of Medicine, Stanford, CA USA

7   94305

8   2 Department of Pediatrics, Stanford School of Medicine, Stanford, CA USA 94305

9   3 Neuroscience Institute, NYU Grossman School of Medicine, New York, NY USA 10016

10   4 Department of Neuroscience and Physiology, NYU Grossman School of Medicine, New York,

11   NY, USA 10016

12   5 Department of Ophthalmology, NYU Grossman School of Medicine, New York, NY, USA

13   10016

14   6 Parekh Center for Interdisciplinary Neurology, NYU Grossman School of Medicine, New York,

15   NY, USA 10016

16   7 Center for Cancer Cellular Therapy, Stanford School of Medicine, Stanford, CA USA 94305

17   8 Howard Hughes Medical Institute, Stanford University, Stanford, CA USA 94305

18   *co-first authors

19   Correspondence should be addressed to: Michelle Monje mmonje@stanford.edu

20   Lead author: Michelle Monje

Summary

Persistent central nervous system (CNS) immune dysregulation and consequent dysfunction of multiple neural cell types is central to the neurobiological underpinnings of a cognitive impairment syndrome that can occur following traditional cancer therapies or certain infections. Immunotherapies have revolutionized cancer care for many tumor types, but the potential long-term cognitive sequelae are incompletely understood. Here, we demonstrate in mouse models that chimeric antigen receptor (CAR) T cell therapy for both CNS and non-CNS cancers can impair cognitive function and induce a persistent CNS immune response characterized by white matter microglial reactivity and elevated cerebrospinal fluid (CSF) cytokines and chemokines. Consequently, oligodendroglial homeostasis and hippocampal neurogenesis are disrupted. Microglial depletion rescues oligodendroglial deficits and cognitive performance in a behavioral test of attention and short-term memory function. Taken together, these findings illustrate similar mechanisms underlying immunotherapy-related cognitive impairment (IRCI) and cognitive impairment following traditional cancer therapies and other immune challenges.

Introduction

Cancer therapy-related cognitive impairment (CRCI) affects a large number of cancer survivors[1]. Traditional cancer therapies are frequently associated with a syndrome of persistent cognitive impairment characterized by deficits in memory, attention, speed of information processing, multitasking, and executive function[1,2]. While best described after traditional therapies like cytotoxic chemotherapy[1], early reports suggest that immunotherapies may also increase the risk of persistent cognitive symptoms[3-5] (for review see[6]). Cancer therapies such as cranial irradiation [7-10] or methotrexate chemotherapy[11,12,13], can induce a reactive state in microglia, particularly in a subpopulation of microglia that reside in axon tracts[14] such as in subcortical white matter[11]. These reactive microglia impair myelin homeostasis[11,15] and plasticity[12], as well as hippocampal

46 neurogenesis[7,8] through mechanisms that include cytokine signaling[8] and induction of neurotoxic

47 astrocyte substates[11,16]. Respiratory viral infections such as COVID and influenza, which can

48 cause a cognitive syndrome that mirrors CRCI, induce a state of microglial reactivity associated

49 with impairments in the same mechanisms of neural homeostasis and plasticity that are

50 dysregulated after cancer therapies[15]. As microglial reactivity is central to several mechanisms

51 underpinning cognitive impairment after traditional cancer therapies (for review, please see[17]), we

52 hypothesized that immunotherapies - primarily inflammatory in mechanism - may similarly induce

53 neuroinflammation, consequent dysregulation of neural cells, and cognitive impairment.

54

55 CAR T cell therapy has been transformative for refractory hematological malignancies in both

56 children and adults, and CD19-targeting CAR T cells are now FDA-approved for treatment of

57 acute lymphoblastic leukemias as well as other hematological cancers[18]. Recently, the

58 disialoganglioside GD2 was found to be a promising target for a lethal high-grade glioma of

59 childhood called H3K27M-altered diffuse midline glioma, also called diffuse intrinsic pontine

60 glioma (DIPG) for tumors of the brainstem[19], and early clinical trial (NCT04196413) results testing

61 GD2-targeting CAR T cells for DIPG have been encouraging[20]. CAR T cell therapy has been

62 associated with acute neurotoxicity syndromes such as immune effector cell-associated

63 neurotoxicity (ICANS)[21,22], but the longer-term consequences are understudied. To assess the

64 neurobiological consequences of CAR T cell therapy after the acute period of tumor clearance,

65 we tested the chronic effects of CAR T-cell immunotherapy for malignancies within and outside

66 of the nervous system on CNS immune state, myelin homeostasis, hippocampal neurogenesis,

67 and cognitive function in preclinical mouse models.

68

69 **Results:**

70 **Impaired cognition in mice after tumor-clearing CAR T cell therapy**

71 To determine whether mice treated with CAR T cell therapy exhibit cognitive deficits, we

72 utilized patient-derived xenograft murine models of CNS and non-CNS cancers (Figure 1A).

73 These models include: an H3K27M+ diffuse intrinsic pontine glioma (DIPG) model, a pre-B cell

74 acute lymphoblastic leukemia (ALL) model, and two osteosarcoma models. Of the two

75 osteosarcoma models, one osteosarcoma model clears efficiently and is associated with minimal

76 cytokine release with CAR T cell therapy (henceforth referred to as "rapid-clearing

77 osteosarcoma"), and one osteosarcoma model is more aggressive, is engineered to express

78 CD19 for experimental CAR T cell studies, and is associated with high cytokine release with CAR

79 T cell therapy (henceforth referred to as "aggressive osteosarcoma")[23,24]. These models were

80 chosen to control for tumor location (DIPG is within the CNS, ALL is primarily outside of but can

81 involve the CNS, and osteosarcoma is exclusively outside of the CNS), CAR T cell target (GD2,

82 CD19 or B7H3), and degree of cytokine release associated with tumor clearance (Figures 1A-

83 1E). Pairs of tumor type and on-target therapeutic (tumor-clearing) CAR T cell are as follows:

84 DIPG with GD2-CAR T[19], ALL with CD19-CAR T[25], aggressive osteosarcoma (engineered to

85 express CD19)[24] with CD19-CAR T, and rapid-clearing osteosarcoma with either GD2- or B7H3-

86 CAR T. All CAR T cell constructs contain the 4-1BBz co-stimulatory domains[24,26]. Tumor

87 clearance timelines varied across models and are as shown in Figures 1B-1E. All experiments

88 were performed with a mock T cell control, for which tumor-bearing mice received T cells which

89 were identically manipulated and activated but do not express a CAR construct. In the DIPG and

90 ALL models, we included an additional off-target CAR T-cell control group that does not treat the

91 tumor in that model and controls for possible effects of these CAR T cells (CD19- and GD2-

92 targeting) on normal tissues.

93 Early clinical reports suggest that a substantial fraction of patients exhibit long-term

94 neurological sequelae by ~one year after CAR T cell therapy, including difficulties with attention

95 and memory[3,4]. We therefore tested these cognitive functions in our murine models using a

96 modified novel object recognition test (NORT) to assess for deficits in attention and short term

97 (<5min) memory (Figure 1F). Mice treated with tumor-clearing CAR T cells in the patient-derived

98 DIPG model, ALL model, and aggressive osteosarcoma model each exhibited impaired

99 behavioral performance in the novel object recognition test, indicating attention and/or memory

100 deficits (Figure 1G-1I). In contrast, tumor-bearing mice treated with off-target GD2-CAR T cells,

101 off-target CD19-CAR T cells, or mock T cells, exhibit intact behavioral performance in novel object

102 recognition testing (Figure 1G-1I).

103   Notably, in the second osteosarcoma model that clears rapidly with CAR T cell therapy,

104 mice treated with either tumor-clearing GD2- or B7H3-CAR T cells demonstrate no cognitive

105 behavioral deficits in novel object recognition testing (Figure 1J), suggesting intact cognition

106 following this relatively efficient CAR T cell-mediated tumor clearance.

107   To further investigate cognitive performance and specifically assess hippocampal-related

108 spatial working memory, we used the Spontaneous Alternation T Maze Test (Figure 1K). This

109 task is a well-established test of spatial memory that requires intact hippocampal function[27,28]. We

110 found that mice bearing xenografts of DIPG, ALL, or aggressive osteosarcoma and treated with

111 tumor-clearing CAR T cells were unable to adequately perform the T Maze Test (Figure1L-1N).

112 Tumor-bearing mice treated with mock T cells did exhibit adequate performance in the T Maze

113 test (Figures 1L-1O), suggesting that the presence of tumor alone does not account for impaired

114 hippocampal-dependent spatial memory function. In contrast to the cognitive performance in the

115 first three models, the rapid-clearing osteosarcoma model shows intact cognitive performance in

116 the T Maze after tumor-clearing CAR T cell therapy (Figure 1O), consistent with the NORT results

117 above and underscoring that cognitive impairment is not associated with tumor-clearing CAR T

118 cell therapy in every case. Taken together, these NORT and T Maze behavioral data demonstrate

119 impaired cognitive function in both CNS and non-CNS cancer models following tumor-clearing

120 CAR T cell therapy (Figures 1G-1I and 1L-1N) that is not explained by the presence of tumor nor

121 on-target, off-tumor effects of the CAR T cells.

122

123 **Persistent CSF cytokine and chemokine elevation after tumor-clearing CAR T cell therapy**

124   To assess the blood and CSF cytokine and chemokine profiles in each tumor model

125 following CAR T cell therapy, we collected cerebrospinal fluid (CSF) ~one month following

126 therapeutic CAR T cell or mock T cell control administration and measured cytokines and

127 chemokines. At one month following tumor-clearing CAR T cell administration, CSF cytokines

128 were elevated above the levels seen in tumor-bearing, mock T cell-treated controls in the DIPG,

129 ALL and aggressive osteosarcoma models (Figure 2A-2C), but not in the rapid-clearing

130 osteosarcoma model (Figure 2D). Prominently, we observed persistently elevated levels of

131 eotaxin/CCL11, CCL2, CCL7, CXCL1, CXCL10 and BAFF in the DIPG, ALL, and aggressive

132 osteosarcoma models (Figure 2A-2C), the same three models that also exhibit cognitive deficits

133 (Figure 1). Eotaxin/CCL11 is of particular interest as it is a chemokine sufficient to cause cognitive

134 impairment, microglial reactivity in the hippocampus and reduced hippocampal neurogenesis[15,29].

135 To better understand why mice treated for rapid-clearing osteosarcoma may not exhibit elevated

136 cytokine/chemokine levels in the CSF we also examined serum cytokines and chemokines in the

137 two osteosarcoma models (Fig S1). At one month following tumor-clearing CAR T cell therapy,

138 the aggressive osteosarcoma model exhibited persistently elevated serum levels of CCL11, CCL2

139 and BAFF compared to tumor-bearing, mock T cell-treated control mice (Fig S1A-S1B). In

140 contrast, the rapid-clearing osteosarcoma model does not exhibit significantly elevated levels of

141 any measured cytokine (Fig S1A-S1B) in the serum. This raises the possibility that CAR T cell

142 therapy in this cognitively intact model does not elicit a similar immune response during the CAR

143 T cell-mediated tumor-clearing process as the cognitively impaired models, suggesting that it is

144 not the CAR T cell-tumor interaction per se but rather a broader accompanying immune response

145 that triggers CNS immune dysregulation.

146

147 **Persistent white matter microglial reactivity after tumor-clearing CAR T cell therapy**

148   Previous work has demonstrated that a wide variety of both CNS-directed and systemic

149 insults can induce reactivity of microglia, the CNS-resident tissue macrophages, especially in

150 white matter regions[8,11,15]. We therefore set out to evaluate the presence and distribution of

151 microglial reactivity following CAR T cell therapy in the various CAR T cell therapy models used

152 here. We assessed microglial number (assessed by positivity for the pan-microglial marker Iba1)

153 and reactivity (assessed by Iba1, CD68 co-positivity) of microglia in the cortex, subcortical white

154 matter, and white matter of the hippocampal dentate gyrus. Both microglial numbers and reactivity

155 were increased in subcortical white matter and hippocampal white matter after tumor-clearing

156 CAR T cell therapy for DIPG xenografted to the brainstem (Figures 3A-3B; S2A-S2B). Microglial

157 number but not reactivity was also increased in the cortex after tumor-clearing CAR T cell therapy

158 for DIPG (Figure 3C; S2C). Following tumor-clearing CAR T cell therapy for ALL, we found

159 increased microglial reactivity in the subcortical white matter, increased microglial numbers and

160 reactivity in the hippocampal white matter, and no changes in cortical microglia (Figures 3D-3F;

161 S2D-S2F). The aggressive osteosarcoma model exhibits an increase in microglial number and

162 reactivity in subcortical white matter, increased microglial reactivity in the hippocampal white

163 matter, and no changes in cortical microglia following tumor-clearing CAR T cell therapy (Figures

164 3G-3I; S2G-S2I). In the rapid-clearing osteosarcoma model with intact cognitive behavioral

165 performance, neither GD2- nor B7H3-targeting, tumor-clearing CAR T cell therapy resulted in an

166 increase in microglial number or reactivity in any of the regions evaluated (Figure 3J-3L; S2J-

167 S2L). Microglia were not elevated in off-target control groups in any model, indicating that on-

168 target, off-tumor effects of the CAR T cells do not account for the microglial changes observed in

169 the tumor-clearing CAR T cell groups. Taken together, these data illustrate persistent reactivity

170 chiefly involving white matter microglia following tumor-clearing CAR T cell therapy in the mouse

171 models that also exhibit cognitive behavioral deficits and CSF cytokine/chemokine elevation.

172

173 **Tumor-clearing CAR T cell therapy can disrupt oligodendroglial lineage cell dynamics**

174   Microglial reactivity can dysregulate oligodendroglial homeostasis and plasticity[11,12]. To

175   assess oligodendroglial integrity after CAR T cell therapy, we quantified oligodendrocyte

176   precursor cells (OPCs) and mature oligodendrocytes in the cortex and subcortical white matter.

177   In the cortex, we found no changes after tumor-clearing or off-target CAR T cell administration in

178   any of the models (Figure S3A-S3H). However, subcortical white matter exhibited a marked

179   decrease in both OPCs (20-25% decrease, Figures 4A-4C) and oligodendrocytes (25-35%

180   decrease, Figures 4D-4F) at one month following tumor-clearing CAR T cell administration in

181   each of the DIPG, ALL and aggressive osteosarcoma models, compared to tumor-bearing mock

182   T cell and off-target CAR T cell controls (Figures 4A-4F). The rapid-clearing osteosarcoma model

183   showed no changes in OPCs or oligodendrocytes after tumor-clearing GD2 or B7H3-CAR T cell

184   treatment (Figures 4G and 4H), concordant with the lack of microglial reactivity, CSF cytokine

185   elevation or cognitive behavioral deficits in this model as described above.

186   This reduction in mature oligodendrocytes suggests potential disruption of myelin

187   homeostasis. To assess myelin ultrastructure, we performed transmission electron microscopy

188   (TEM) of the subcortical white matter (cingulum of the corpus callosum). We found a ~20%

189   decrease in subcortical white matter myelinated axon density following GD2-CAR T cell clearance

190   of DIPG xenografted to the brainstem in comparison to mock T cell-treated, tumor-bearing

191   controls (Figures 4I-4J). No significant difference was observed in myelin sheath thickness (g-

192   ratio) between groups (Figure S3I-S3J).

193

194   **Tumor-clearing CAR T cell therapy can impair hippocampal neurogenesis**

195   Reactive microglia and particular cytokines/chemokines, including CCL11, can impair

196   hippocampal neurogenesis[8,15,29,30], an important component of neural plasticity that contributes to

197   spatial memory function[31-34]. Given the observed increase in dentate gyrus white matter reactive

198   microglia and in CCL11 and other CSF cytokines/chemokines, together with spatial memory

199   deficits, we hypothesized that neurogenesis may be impaired following tumor-clearing CAR T cell

200   administration.

201   We next investigated neurogenesis in the dentate gyrus of the hippocampus by quantifying

202   doublecortin-positive neuroblasts[35,36]. We found that neurogenesis is diminished by 40-50%

203   following tumor-clearing CAR T cell therapy in the DIPG, ALL, and aggressive osteosarcoma

204   models, compared to off-target CAR T or mock T cell controls (Figure 5A-5C). Interestingly, the

205   rapid-clearing osteosarcoma model exhibited a small increase in neurogenesis following tumor-

206   clearing B7H3-CAR T cell administration, but was at control levels following tumor-clearing GD2-

207   CAR T cell administration (Figure 5D). Taken together, these findings are concordant with the

208   emerging pattern of multicellular dysregulation and cognitive impairment following CAR T cell

209   therapy that induces persistent neuroinflammation.

210

211   **Anti-cytokine therapy targeting IL1a does not rescue cognitive performance**

212   Anti-cytokine agents such as Anakinra, an interleukin-1 receptor antagonist, are frequently

213   administered to CAR T cell patients to treat acute neurotoxicity such as immune effector cell-

214   associated neurotoxicity (ICANS) frequently seen in patients with ALL[37,38]. We therefore assessed

215   the possible effects of Anakinra on the observed cellular dysregulation and cognitive deficits in

216   the ALL model to assess possible rescue of cellular homeostasis and cognitive behavior after

217   tumor-clearing CAR T cell therapy. Anakinra was administered (10 mg/kg i.p.) from day 0 to day

218   14 of CAR T cell treatment (Figure S4A). We found no effects on Anakinra on microglial reactivity,

219   oligodendroglial deficits, hippocampal neurogenesis deficits nor rescue of cognitive performance

220   (Figures S4B-S4F).

221

222   **CSF1R inhibition differentially depletes microglia in subcortical and hippocampal white**

223   **matter**

224   Microglial reactivity and consequent dysregulation of oligodendroglial lineage cells and

225   hippocampal neurogenesis is thought to be central to cognitive impairment following traditional

226   cancer therapies such as radiation and chemotherapy (for review see[17]). Accordingly, microglial

227   depletion rescues cellular and cognitive deficits after traditional cancer therapies[11,39]. Therefore,

228   we tested whether microglial depletion after the period of CAR T cell-mediated tumor clearance

229   could rescue cellular and cognitive impairment in these mouse models.

230   To deplete microglia, we used a small-molecule inhibitor of Colony Stimulating Factor 1

231   Receptor (CSF1R), PLX5622[40]. Most microglia and macrophages depend on CSF1R signaling

232   for survival and therefore, treatment with the CSF1R inhibitor (CSF1Ri) results in swift clearance

233   of the majority of microglia in the brain[41]. Not all microglia are CSF1R-dependent, and a fraction

234   of microglia remain[42]. We administered CSF1Ri formulated in mouse chow from D21 to D35 in

235   the DIPG model (Figure 6A) and from D14 to D28 in the ALL model (Figure 6B). Following 14

236   days of CSF1R inhibitor treatment, microglia were depleted by 70-75% in subcortical white matter

237   (Figure 6C-6D), but only depleted by 45-55% in the hippocampal white matter (Figures 6E-6F),

238   underscoring the regional heterogeneity of microglial subpopulations.

239   In the context of this partial microglial depletion, neither hippocampal neurogenesis nor

240   spatial memory performance were rescued by CSF1R inhibition following tumor-clearing CAR T

241   cell therapy for DIPG or ALL (Figure S5).

242

243   **Microglial depletion rescues oligodendroglial dysregulation and cognitive behavior**

244   Given the more robust depletion of subcortical microglia with CSF1R inhibition, we next

245   tested the role of reactive microglia in the subcortical oligodendroglial dysfunction observed

246   following tumor-clearing CAR T cell therapy. We found that subcortical microglial depletion led to

247   a normalization of oligodendroglial lineage cell populations, with a rescue of OPC and mature

248   oligodendrocyte numbers following tumor-clearing CAR T cell administration in both the DIPG

249   and ALL models (Figure 6G-6J). Together with normalization of myelin-forming cells, microglial

250   depletion rescued cognitive performance in the novel object recognition test of attention and short-

251   term memory following tumor-clearing CAR T cell therapy in both DIPG and ALL models (Figures

252   6K and 6L). In contrast, and consistent with the results above, mice treated with tumor-clearing

253   CAR T cell therapy for either DIPG or ALL who received vehicle did not discern between the novel

254   and familiar object (Figures 6K and 6L). These findings implicate reactive microglia as central to

255   the subcortical oligodendroglial lineage dysregulation and associated cognitive behavioral

256   impairment observed following tumor-clearing CAR T cell therapy.

257

258   **Discussion**

259   Taken together, the findings presented here illustrate persistent neuroinflammatory changes,

260   multi-lineage neural cellular dysregulation and consequent cognitive impairment in multiple

261   mouse models of CAR T cell therapy for CNS and non-CNS malignancies. Concordant with early

262   reports of cognitive deficits in patients years following immunotherapy[3-5] that are clinically similar

263   to those experienced by cancer survivors treated with traditional therapies (for review, see[6]), we

264   find that immunotherapy-related cognitive impairment (IRCI) shares mechanistic underpinnings

265   with cognitive impairment caused by chemotherapy[11-13] and cranial radiation[7-9]. Both traditional

266   and immune-based therapies elicit a consistent pattern of white matter-selective microglial

267   reactivity, consequent disruption of oligodendroglial homeostasis and hippocampal neurogenesis,

268   and impairment in attention and memory function.

269

270   Importantly, control experiments illustrate that on-target, off-tumor effects on normal tissue do not

271   account for the neuroinflammation nor the cellular and behavioral deficits observed in the context

272   of tumor clearance, at least for the specific CAR T cells studied. The GD2 antigen is identical in

273   humans and in mice[43], thus the non-tumor-targeting GD2-CAR-T cell control groups served to

274   control for on-target, off-tumor effects of the human GD2-CAR T cells used in these mouse

275   models. However, it should be noted that CAR T cell reactivity with antigens on normal neural

276 tissues could occur and cause neurological sequelae with different antigen-targeting CAR T cell

277 therapies, as appears may happen with BCMA-targeting CAR T cells[44]. Additionally, while the

278 presence of a tumor alone can cause a degree of CSF cytokine/chemokine elevation, especially

279 for cancers that involve the CNS, the presence of the tumor alone did not account for the microglial

280 reactivity or downstream cognitive effects observed in any of the models studied.

281

282 We find here that while CAR T cell therapy can cause neuroinflammation that triggers a cascade

283 of downstream effects resulting in cognitive dysfunction, it does not always do so. In the rapid-

284 clearing model of osteosarcoma, CAR T cells efficiently clear the cancer and do not elicit

285 neuroinflammatory changes of CSF cytokine/chemokine elevation nor microglial reactivity. This

286 suggests that it is not the CAR T cell interaction with the tumor per se, but rather the broader

287 immune response frequently evoked by anti-tumor CAR T responses that results in these

288 neuropathophysiological changes. While much remains to be learned about how the immune

289 response evoked by tumor-clearing CAR T cell therapy outside of the CNS results in CNS

290 inflammation, a similar phenomenon is observed after certain viral respiratory infections. Infection

291 with SARS-CoV2 or H1N1 influenza that is restricted to the respiratory system also induces CSF

292 cytokine and chemokine elevations and white matter-selective microglial reactivity[15].

293

294 The cognitive deficits that can occur following chemotherapy, immunotherapy, and certain

295 infections such as COVID or influenza share clinical features and neurobiological underpinnings.

296 Microglia in the subcortical white matter, also called axon tract microglia[14], are exquisitely

297 sensitive to immune challenges and toxic exposures and exhibit reactivity following systemic

298 methotrexate chemotherapy[11,12], mild respiratory COVID[15], mild respiratory H1N1 influenza[15], and

299 CAR T cell therapy. In mild respiratory-restricted COVID or influenza mouse models[15], and in the

300 aggressive osteosarcoma model studied here, neuroinflammatory changes are seen in response

301 to immune challenges exclusively outside of the nervous system. How the immune response is

302   relayed from the periphery to the CNS is incompletely understood. Past work demonstrates that

303   circulating chemokines such as CCL11 are sufficient to elicit microglial reactivity and impaired

304   neurogenesis[15,29], but the possible signaling molecules, immune cellular trafficking and/or afferent

305   neural input responsible for the broader neuroinflammatory response remain to be elucidated.

306   However, a range of disease states characterized by a syndrome of impaired attention, memory,

307   speed of information processing and executive function share a consistent pattern of white matter

308   microglial reactivity, multi-lineage cellular dysregulation disrupting neural homeostasis and

309   plasticity, and consequent cognitive impairment. Neural-immune principles of "brain fog"

310   syndromes are thus emerging, and therapeutic strategies developed to mitigate cognitive

311   symptoms for one disease context are likely to apply to many.

312

313   While consistent neuropathophysiological patterns are emerging in the various disease contexts

314   associated with "brain fog" syndromes, important distinctions are also emerging. Comparing

315   myelin changes after respiratory COVID, methotrexate chemotherapy and CAR T cell therapy,

316   myelinated axons are decreased in each case, but only after methotrexate is myelin sheath

317   thickness also affected. Comparing respiratory infections with SARS-CoV2 or H1N1 influenza,

318   white matter microglial reactivity and oligodendroglial dysregulation were evident at 7 days in both

319   and resolved by 7 weeks after influenza but remained aberrant at 7 weeks after SARS-CoV2

320   infection. Comparing cytokine and chemokine profiles in the CSF after these two respiratory viral

321   infections reveals both shared and distinct patterns of persistent elevation. Similarly, comparing

322   CSF cytokine/chemokine elevations in aggressive osteosarcoma and ALL models following

323   tumor-clearing CAR T cell therapy here, many shared but also some distinct changes are

324   observed, such as elevated CCL7 and BAFF in the ALL model but not the aggressive

325   osteosarcoma model. Finally, important distinctions between subpopulations of microglia are

326   important to recognize. While white matter microglia are uniquely sensitive to various toxic and

327   immune challenges, microglia in hippocampal white matter are further distinguished by differential

328   sensitivity to CCL11[15] and resistance to CSF1Ri-mediated clearance.

329

330   **Limitations of the Study**

331   An important caveat of this study is the use of immunocompromised mouse models. While this

332   enabled evaluation of the CAR T cells used in the clinic and patient-derived tumors, these mice

333   lack endogenous lymphocytes, and while myeloid cells are present these are not educated by

334   lymphocytes as would normally occur in an immunocompetent mouse[45]. The full immune

335   response elicited by tumor-clearing CAR T cell therapy may therefore not be appreciated here.

336   Another important caveat of studying patient-derived xenograft models treated with human CAR

337   T cells is that graft-versus-host disease develops after approximately 6 weeks, so longer term

338   effects on cognition could not be studied here. A remaining question is thus how long the cellular

339   dysregulation and cognitive impairment may persist beyond the timepoints assessed here.

340

341   Additional mechanisms implicated in cancer therapy-related cognitive impairment, and future

342   studies should explore the role these mechanisms may play in ICRI. In addition to oligodendroglial

343   and myelin dysregulation, reactive microglia can also induce neurotoxic substates of

344   astrocytes[16,46], which may cause cell death of oligodendrocytes and susceptible neurons, as well

345   as impair normal astrocytic support of synapses[16]. Such astrocyte reactivity has been described

346   following methotrexate chemotherapy in mice, and might explain the loss of oligodendroglial

347   homeostasis observed here after CAR T cell therapy. Impaired synaptic connectivity and plasticity

348   can be another consequence of traditional cancer therapies[47-49], and should be explored in future

349   studies of IRCI. Finally, chemotherapy-induced choroid plexus dysfunction may alter the

350   antioxidant properties of CSF and contribute to cognitive impairment

351   [50]. Whether similar such alterations in choroid plexus biology and consequent changes to CSF

352   supportive and neurotrophic functions[51] are induced by immunotherapy remains to be determined.

353

354 **Conclusions** CAR T cell therapy has been transformative for hematological malignancies and

355 holds enormous promise for solid tumors. Understanding the potential cognitive sequelae of the

356 immune response associated with tumor-clearing CAR T-cell therapy and the

357 neuroimmunological underpinnings of these possible neurological consequences is of paramount

358 importance to optimizing quality of life for survivors. Given the mechanistic parallels evident in

359 cognitive impairment syndromes that follow a range of inflammatory disease states, such

360 progress may enable therapeutic interventions for many living with persistent "brain fog"

361 syndromes.

362

363

375

376 **Author Contributions**

377 Conceptualization, methodology, validation, and visualization were performed by

378   M.M., R.G.M., A.C.G., L.A-A.; formal analysis by A.C.G., L.A-A., M.O'D; resources provided by

379   M.M., R.G.M.; investigation was performed by A.C.G., L.A-A., M.R., S.D., R.M., K.S.; writing –

380   original draft by M.M. and L.A-A; writing – review & editing by M.M., A.C.G., L.A-A, K.S.; data

381   curation by A.C.G., L.A-A.; supervised by M.M., S.A.L., R.G.M.; funding acquisition by M.M.,

382   S.A.L., R.G.M

383

384   **Declaration of Interests** M.M. holds equity in MapLight and CARGO Life Sciences. M.M. and

385   R.G.M. are inventors on a patent filed by Stanford University relevant to GD2-CAR T cell therapy

386   for DIPG/DMG. R.G.M. is a cofounder of and holds equity in Syncopation Life Sciences; he is

387   also a consultant for Lyell Immunopharma, Syncopation Life Sciences, NKarta, Gamma Delta

388   Therapeutics, Aptorum Group, Illumina Radiopharmaceuticals, ImmunAI, Arovella Therapeutics
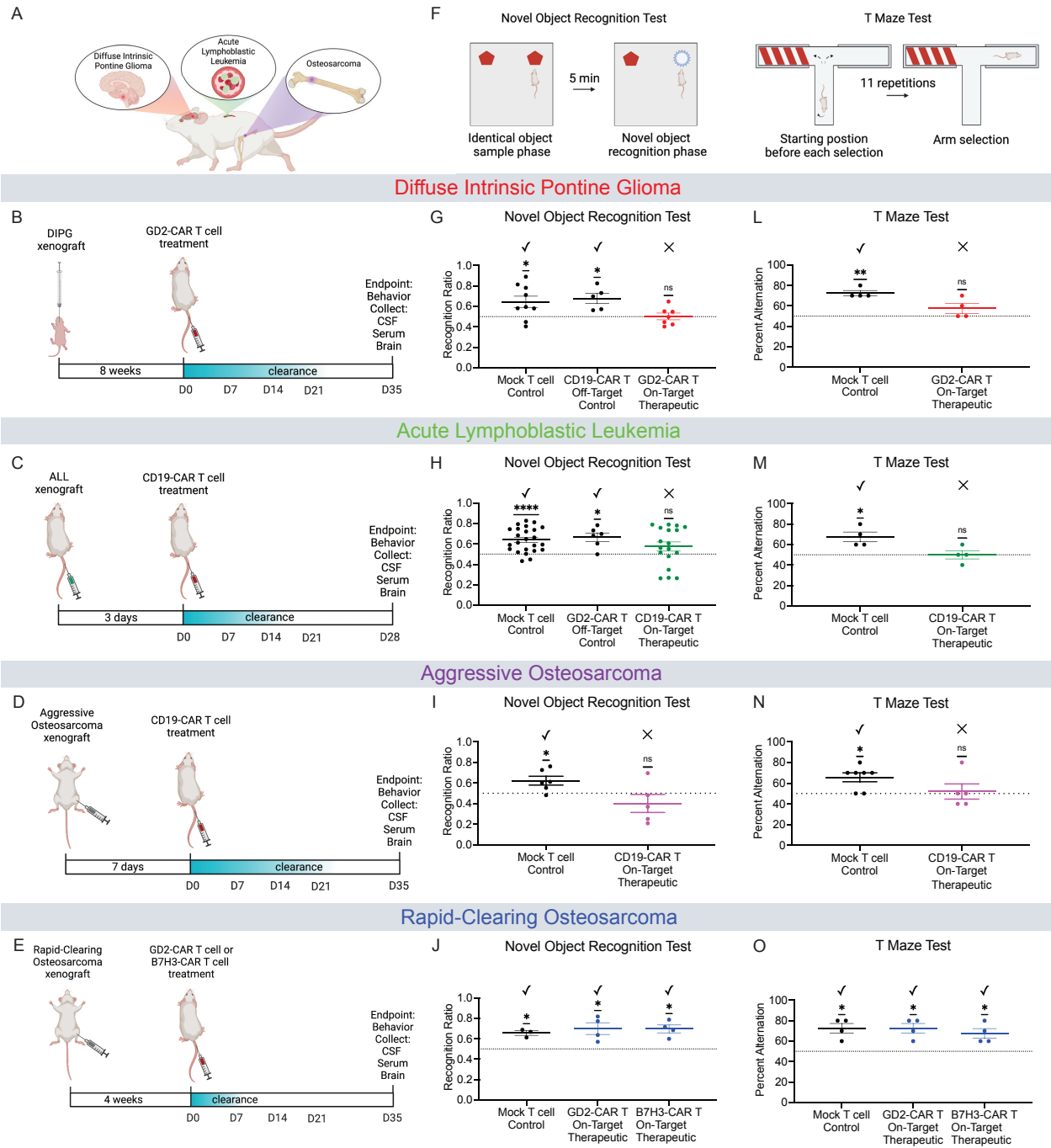
389   and Zai Lab.

390

391

392

393

394

395

396

397

398

399

400

401

402

403

404 **Figures**

405

406 **Figure 1. Cognitive deficits and neuroinflammation following tumor-clearing CAR T cell**
407 **therapy**
408
409 (A) Schematic illustration denoting the murine xenograft models assessed.
410 (B, C, D, E) Schematic illustration of the various xenograft and CAR T cell therapy experimental
411 timelines.

(F) Schematic illustration of the Novel Object Recognition Test (NORT) to evaluate attention and short-term memory. Recognition ratio is defined as the percent time spent with the novel object over the total time spent interacting with either object.

(G) DIPG xenografted mice treated with either mock T cells, Off-Target CD19-CAR T cells, or On-Target Therapeutic GD2-CAR T cells. NORT performed on day 34 post-CAR T therapy. Mock T cell Control (n=9 mice), CD19-CAR T Control (n=5 mice), GD2-CAR T Therapeutic (n=7 mice).

(H) ALL xenografted mice treated with either mock T cells, Off-Target GD2-CAR T cells, or On-Target Therapeutic CD19-CAR T cells. NORT performed on day 27 post-CAR T therapy. Mock T cell Control (n=24 mice), GD2-CAR T Control (n=6 mice), CD19-CAR T Therapeutic (n=18 mice).

(I) Aggressive osteosarcoma xenografted mice treated with either mock T cells or On-Target Therapeutic CD19-CAR T cells. NORT performed on day P34 post-CAR T therapy. Mock T cell Control (n=6 mice), CD19-CAR T Therapeutic (n=5 mice).

(J) Rapid-clearing osteosarcoma xenografted mice treated with either mock T cells, On-Target Therapeutic GD2-CAR T, or On-Target Therapeutic B7H3-CAR T cells. NORT performed on day 34 post-CAR T therapy. Mock T cell Control (n=3 mice), GD2-CAR T Therapeutic (n=4 mice), B7H3-CAR T Therapeutic (n=4 mice).

(K) T Maze Alternation Test to assess spatial working memory and hippocampal-related cognitive dysfunction. Percent Alternation is calculated over 11 trials allowing for 10 decisions.

(L) DIPG xenografted mice treated with either mock T cell Control or On-Target Therapeutic GD2-CAR T cells. T maze performed on day 35 post-CAR T therapy. Mock T cell control (n=4 mice), GD2-CAR T therapeutic (n=4 mice).

(M) ALL xenografted mice treated with either mock T cell Control or On-Target Therapeutic CD19-CAR T cells. T maze performed on day 28 post-CAR T therapy. Mock T cell control (n=4 mice), CD19-CAR T therapeutic (n=4 mice).

(N) Aggressive osteosarcoma xenografted mice treated with either mock T cell Control or On-Target Therapeutic CD19-CAR T cells. T maze performed on day 35 post-CAR T therapy. Mock T cell control (n=7 mice), CD19-CAR T therapeutic (n=5 mice).

(O) Rapid-clearing osteosarcoma xenografted mice treated with either mock T cells, On-Target Therapeutic GD2-CAR T, or On-Target Therapeutic B7H3-CAR T cells. T Maze performed on day 35 post-CAR T therapy. Mock T cell Control (n=4 mice), GD2-CAR T Therapeutic (n=4 mice), B7H3-CAR T Therapeutic (n=4 mice).

(G-J and L-O) Data shown as mean ± SEM. Each point = one mouse. ns = $p > 0.05$, *$p < 0.05$, **$p < 0.01$, ****$p < 0.0001$. Analyzed via One Sample T and Wilcoxon Test.
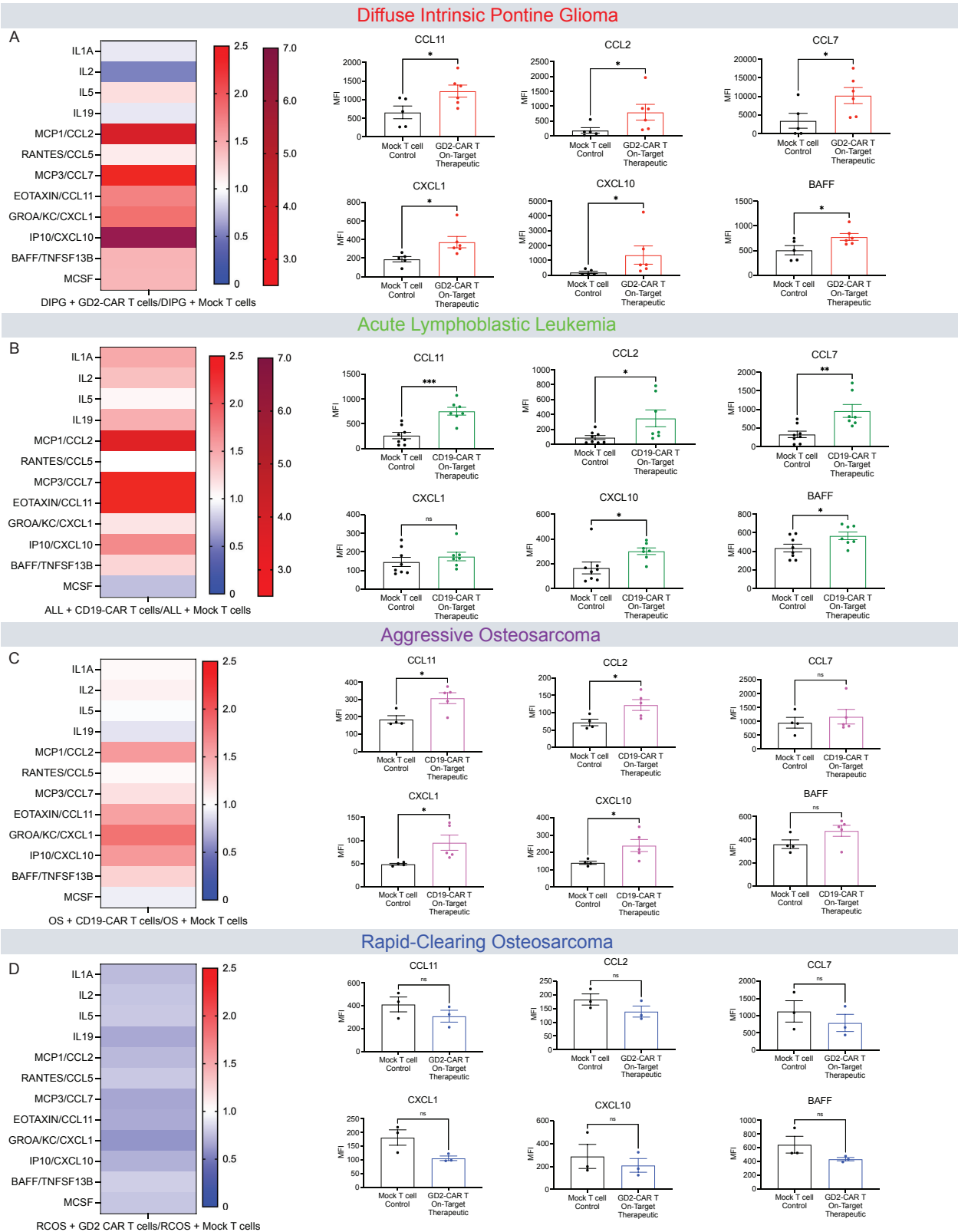
Figure 2. Persistent CSF cytokine and chemokine elevation after tumor-clearing CAR T cell therapy

452 (A) Left, heat map of fold change of cytokine and chemokine analysis of CSF in DIPG+On-Target
453 Therapeutic GD2-CAR T cell treated mice relative to DIPG+mock T cell treated control mice 35-
454 days post-CAR T cell therapy. Right, quantification of raw MFI of CSF levels of cytokines (CCL11,
455 CCL2, CCL7, CXCL1, CXCL10, BAFF).
456 (B) Left, heat map of fold change of cytokine and chemokine analysis of CSF in ALL+On-Target
457 Therapeutic CD19-CAR T cell treated mice relative to ALL+mock T cell treated control mice 28-
458 days post-CAR T cell therapy. Right, quantification of raw MFI of CSF levels of cytokines (CCL11,
459 CCL2, CCL7, CXCL1, CXCL10, BAFF).
460 (C) Left, heat map of fold change of cytokine and chemokine analysis of CSF in aggressive
461 osteosarcoma (OS)+On-Target Therapeutic CD19-CAR T cell treated mice relative to aggressive
462 osteosarcoma (OS)+mock T cell treated control mice 35-days post-CAR T cell therapy. Right,
463 quantification of raw MFI of CSF levels of cytokines (CCL11, CCL2, CCL7, CXCL1, CXCL10,
464 BAFF).
465 (D) Left, heat map of fold change of cytokine and chemokine analysis of CSF in rapid-clearing
466 osteosarcoma (RCOS)+On-Target Therapeutic GD2-CAR T cell treated mice relative to rapid-
467 clearing osteosarcoma (RCOS)+mock T cell treated control mice 35-days post-CAR T cell
468 therapy. Right, quantification of raw MFI of CSF levels of cytokines (CCL11, CCL2, CCL7, CXCL1,
469 CXCL10, BAFF).
470 (A-D) Cytokine and chemokines significantly elevated or depressed, analyzed via Student's T test
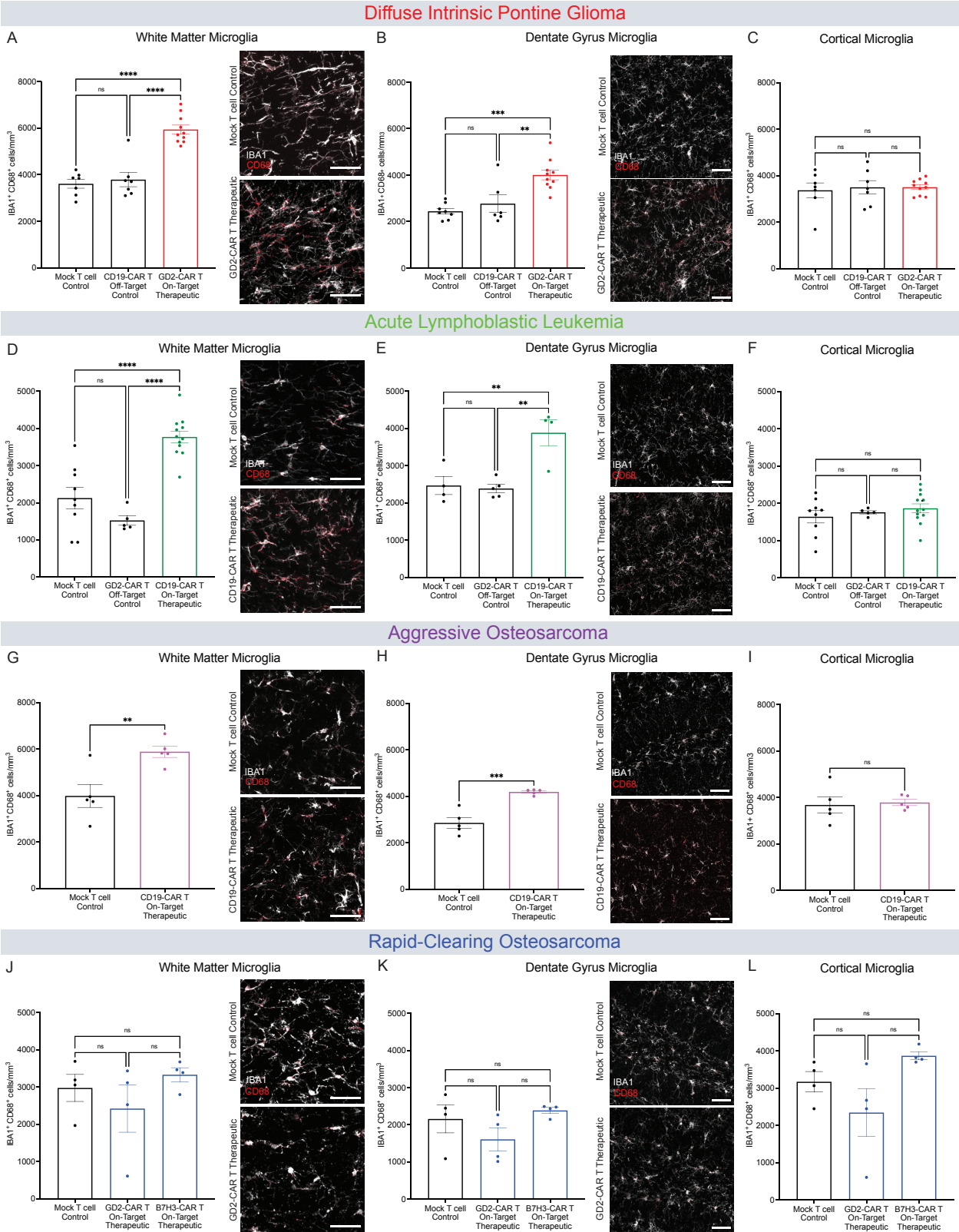471 of raw MFI values.
472

Figure 3. Tumor-clearing CAR T Cell therapy can result in white matter microglial reactivity
(A) Quantification of DIPG xenografted mice microglial reactivity (IBA1+ CD68+) and representative confocal micrographs (white = IBA1; red = CD68) from the corpus callosum 35

477   days post-CAR T therapy. Mock T cell Control (n=7 mice), CD19-CAR T Control (n=7 mice), GD2-
478   CAR T Therapeutic (n=10 mice).
479   (B) Quantification of DIPG xenografted mice microglial reactivity (IBA1+ CD68+) and
480   representative confocal micrographs (white = IBA1; red = CD68) 35 days post-CAR T cell therapy
481   in the hilar white matter region of the dentate gyrus. Mock T cell Control (n=8 mice), CD19-CAR
482   T Control (n=6 mice), GD2-CAR T Therapeutic (n=10 mice).
483   (C) Quantification of DIPG xenografted mice microglial reactivity (IBA1+ CD68+) 35 days post-
484   CAR T therapy in the cortical grey matter. Mock T cell Control (n=7 mice), CD19-CAR T Control
485   (n=7 mice), GD2-CAR T Therapeutic (n=10 mice).
486   (D) Quantification of ALL xenografted mice microglial reactivity (IBA1+ CD68+) and representative
487   confocal micrographs (white = IBA1; red = CD68) from the corpus callosum 28 days post-CAR T
488   therapy. Mock T cell Control (n=9 mice), GD2-CAR T Control (n=5 mice), CD19-CAR T
489   Therapeutic (n=12 mice).
490   (E) Quantification of ALL xenografted mice microglial reactivity (IBA1+ CD68+) and representative
491   confocal micrographs (white = IBA1; red = CD68;) 28 days post-CAR T cell therapy in the hilar
492   white matter region of the dentate gyrus. Mock T cell Control (n=4 mice), GD2-CAR T Control
493   (n=5 mice), CD19-CAR T Therapeutic (n=4 mice).
494   (F) Quantification of ALL xenografted mice microglial reactivity (IBA1+ CD68+) 28 days post-CAR
495   T therapy in the cortical grey matter. Mock T cell Control (n=9 mice), GD2-CAR T Control (n=5
496   mice), CD19-CAR T Therapeutic (n=12 mice).
497   (G) Quantification of aggressive osteosarcoma xenografted mice microglial reactivity (IBA1+
498   CD68+) and representative confocal micrographs (white = IBA1; red = CD68) from the corpus
499   callosum 35 days post-CAR T therapy. Mock T cell Control (n=5 mice), CD19-CAR T Therapeutic
500   (n=5 mice).
501   (H) Quantification of aggressive osteosarcoma xenografted mice microglial reactivity (IBA1+
502   CD68+) and representative confocal micrographs (white = IBA1; red = CD68) 35 days post-CAR
503   T cell therapy in the hilar white matter region of the dentate gyrus. Mock T cell Control (n=5 mice),
504   CD19-CAR T Therapeutic (n=5 mice).
505   (I) Quantification of aggressive osteosarcoma xenografted mice microglial reactivity (IBA1+
506   CD68+) 35 days post-CAR T therapy in the cortical grey matter. Mock T cell Control (n=5 mice),
507   CD19-CAR T Therapeutic (n=5 mice).
508   (J) Quantification of rapid-clearing osteosarcoma xenografted mice microglial reactivity (IBA1+
509   CD68+) and representative confocal micrographs (white = IBA1; red = CD68) from the corpus
510   callosum 35 days post-CAR T therapy. Mock T cell Control (n=4 mice), GD2-CAR Therapeutic
511   (n=4 mice), B7H3-CAR T Therapeutic (n=4 mice).
512   (K) Quantification of rapid-clearing osteosarcoma xenografted mice microglial reactivity (IBA1+
513   CD68+) and representative confocal micrographs (white = IBA1; magenta = CD68) 35 days post-
514   CAR T cell therapy in the hilar white matter region of the dentate gyrus. Mock T cell Control (n=4
515   mice), GD2-CAR T Therapeutic (n=4 mice), B7H3-CAR T Therapeutic (n=4 mice).
516   (L) Quantification of rapid-clearing osteosarcoma xenografted mice microglial reactivity (IBA1+
517   CD68+) 35 days post-CAR T therapy in the cortical grey matter. Mock T cell Control (n=4 mice),
518   GD2-CAR Therapeutic (n=4 mice), B7H3-CAR T Therapeutic (n=4 mice).
519
520   (A-F, J-L) Data shown as mean ± SEM. Each point = one mouse, ns = $p > 0.05$, **$p < 0.01$, ***p
521   < 0.001, ****$p < 0.0001$, analyzed via One-way ANOVA.
522   (G-I) Data shown as mean ± SEM. Each point = one mouse, ns = $p > 0.05$, **$p < 0.01$, analyzed
523   via Unpaired T Test. Scale bars equal 50um in all confocal images.
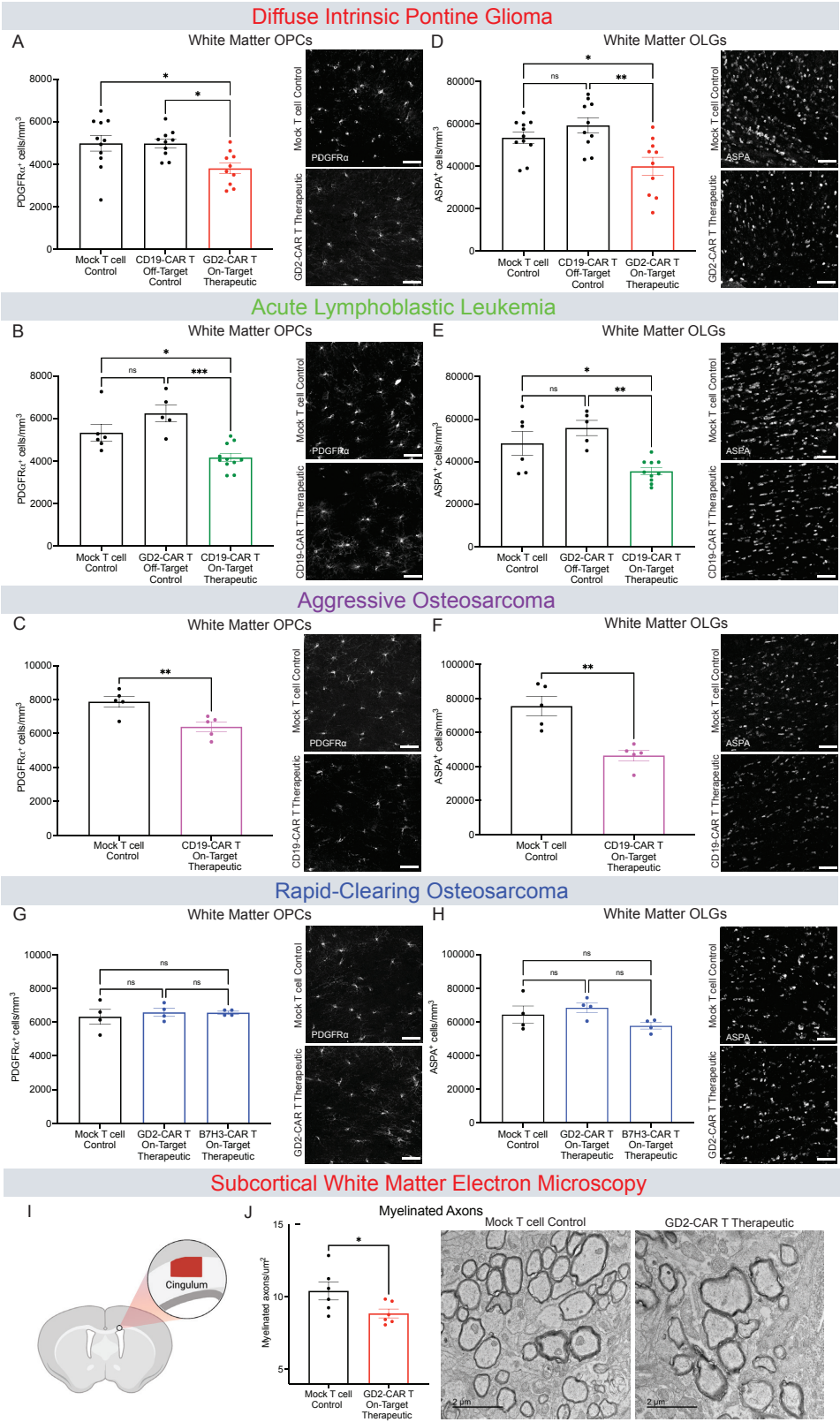524

Figure 4. Tumor-clearing CAR T Cell therapy can result in oligodendroglial and myelin deficits

(A) Quantification and representative confocal micrographs of PDGFRa+ oligodendrocyte precursor cells from the corpus callosum in DIPG xenografted mice 35 days post-CAR T therapy. Mock T cell Control (n=11 mice), CD19-CAR T Control (n=10 mice), GD2-CAR T Therapeutic (n=10 mice).

(B) Quantification and representative confocal micrographs of PDGFRa+ oligodendrocyte precursor cells from the corpus callosum in ALL xenografted mice 28 days post-CAR T therapy. Mock T cell Control (n=6 mice), GD2-CAR T Control (n=5 mice), CD19-CAR T Therapeutic (n=11 mice).

(C) Quantification and representative confocal micrographs of PDGFRa+ oligodendrocyte precursor cells from the corpus callosum in aggressive osteosarcoma xenografted mice 35 days post-CAR T therapy. Mock T cell Control (n=5 mice), CD19-CAR T Therapeutic (n=5 mice).

(D) Quantification and representative confocal micrographs of ASPA+ mature oligodendrocytes from corpus callosum in DIPG xenografted mice 35 days post-CAR T therapy. Mock T cell Control (n=11 mice), CD19-CAR T Control (n=10 mice), GD2-CAR T Therapeutic (n=10 mice).

(E) Quantification and representative confocal micrographs of ASPA+ mature oligodendrocytes from the corpus callosum in ALL xenografted mice 28 days post-CAR T therapy. Mock T cell Control (n=6 mice), CD19-CAR T Control (n=5 mice), GD2-CAR T Therapeutic (n=10 mice).

(F) Quantification and representative confocal micrographs of ASPA+ mature oligodendrocytes from the corpus callosum in aggressive osteosarcoma xenografted mice 35 days post-CAR T therapy. Mock T cell Control (n=5 mice), CD19-CAR T Therapeutic (n=5 mice).

(G) Quantification and representative confocal micrographs of PDGFRa+ oligodendrocyte precursor cells from the corpus callosum in rapid-clearing osteosarcoma xenografted mice 35 days post-CAR T therapy. Mock T cell Control (n=4 mice), GD2-CAR T Therapeutic I (n=4 mice), B7H3-CAR T Therapeutic (n=4 mice).

(H) Quantification and representative confocal micrographs of ASPA+ mature oligodendrocytes from the corpus callosum in rapid-clearing osteosarcoma xenografted mice 35 days post-CAR T therapy. Mock T cell Control (n=4 mice), GD2-CAR T Therapeutic (n=4 mice), B7H3-CAR T Therapeutic (n=4 mice).

(I) Schematic illustration denoting the cingulum region of the corpus callosum used for the transmission electron microscopy (TEM) DIPG xenografted mice 35 days post-CAR T therapy.

(J) Quantification and Representative TEM images of white matter myelinated axons per area at day P35 post-CAR T therapy. Myelinated axonal projections are in cross section and visible as electron-dense sheaths encircling axons. Scale bar = 2 um. Mock T cell control (n=6 mice), GD2-CAR T therapeutic (n=6 mice).

(A, B, D, E, G and H) Data shown as mean ± SEM. Each point = one mouse. ns = p > 0.05, *p < 0.05, **p < 0.01, ***p < 0.001, analyzed via One-way ANOVA.

(C, F and J) Data shown as mean ± SEM. Each point = one mouse, *p < 0.05, analyzed via Unpaired T Test. Scale bars equal 50um in all confocal micrographs (A-H), and 2um in electron microscopy images (J).
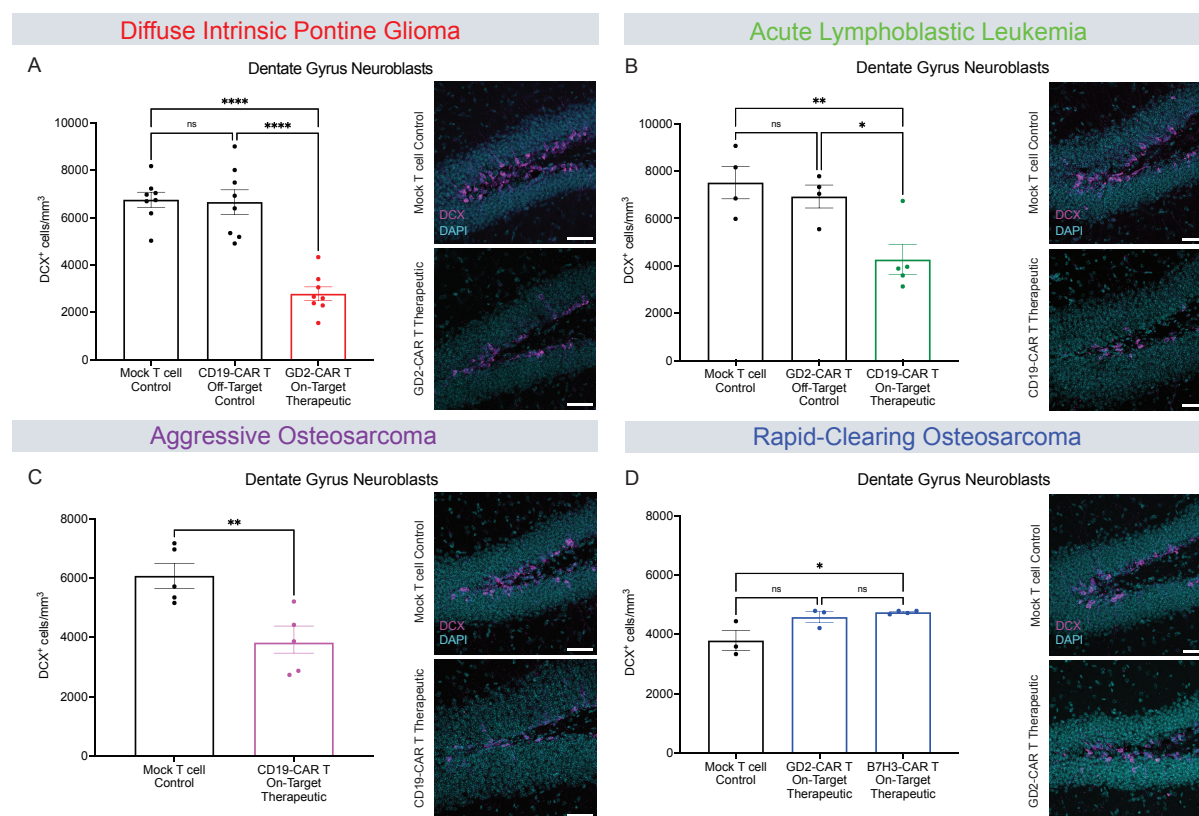
Figure 5. Tumor-clearing CAR T Cell therapy can impair hippocampal neurogenesis

(A) Quantification of neuroblasts (DCX+) in DIPG model and representative confocal micrographs (magenta = DCX; cyan = DAPI) from the dentate gyrus 35 days after CAR T cell therapy. Mock T cell control (n=8 mice), CD19-CAR T control (n=8 mice), GD2-CAR T Therapeutic (n=8 mice).

(B) Quantification of neuroblasts (DCX+) in ALL model and representative confocal micrographs (magenta = DCX; cyan = DAPI) from the dentate gyrus 28 days after CAR T cell therapy. Mock T cell control (n=4 mice), GD2-CAR T control (n=4 mice), CD19-CAR T Therapeutic (n=5 mice).

(C) Quantification of neuroblasts (DCX+) in aggressive osteosarcoma model and representative confocal micrographs (magenta = DCX; cyan = DAPI) from the dentate gyrus 35 days after CAR T cell therapy. Mock T cell control (n=5 mice), CD19-CAR T Therapeutic (n=5 mice).

(D) Quantification of neuroblasts (DCX+) in rapid-clearing osteosarcoma model and representative confocal micrographs (magenta = DCX; cyan = DAPI) from the dentate gyrus 35 days after CAR T cell therapy. Mock T cell control (n=3 mice), GD2-CAR T Therapeutic (n=3 mice), B7H3-CAR T Therapeutic (n=4 mice).

(A, B, and D) Data shown as mean ± SEM. Each point = one mouse. ns = $p > 0.05$, *$p < 0.05$, **$p < 0.01$, ****$p < 0.0001$, analyzed via One-way ANOVA.

(C) Data shown as mean ± SEM. Each point = one mouse, **$p < 0.01$, analyzed via Unpaired T Test. Scale bars equal 50um in all confocal images.
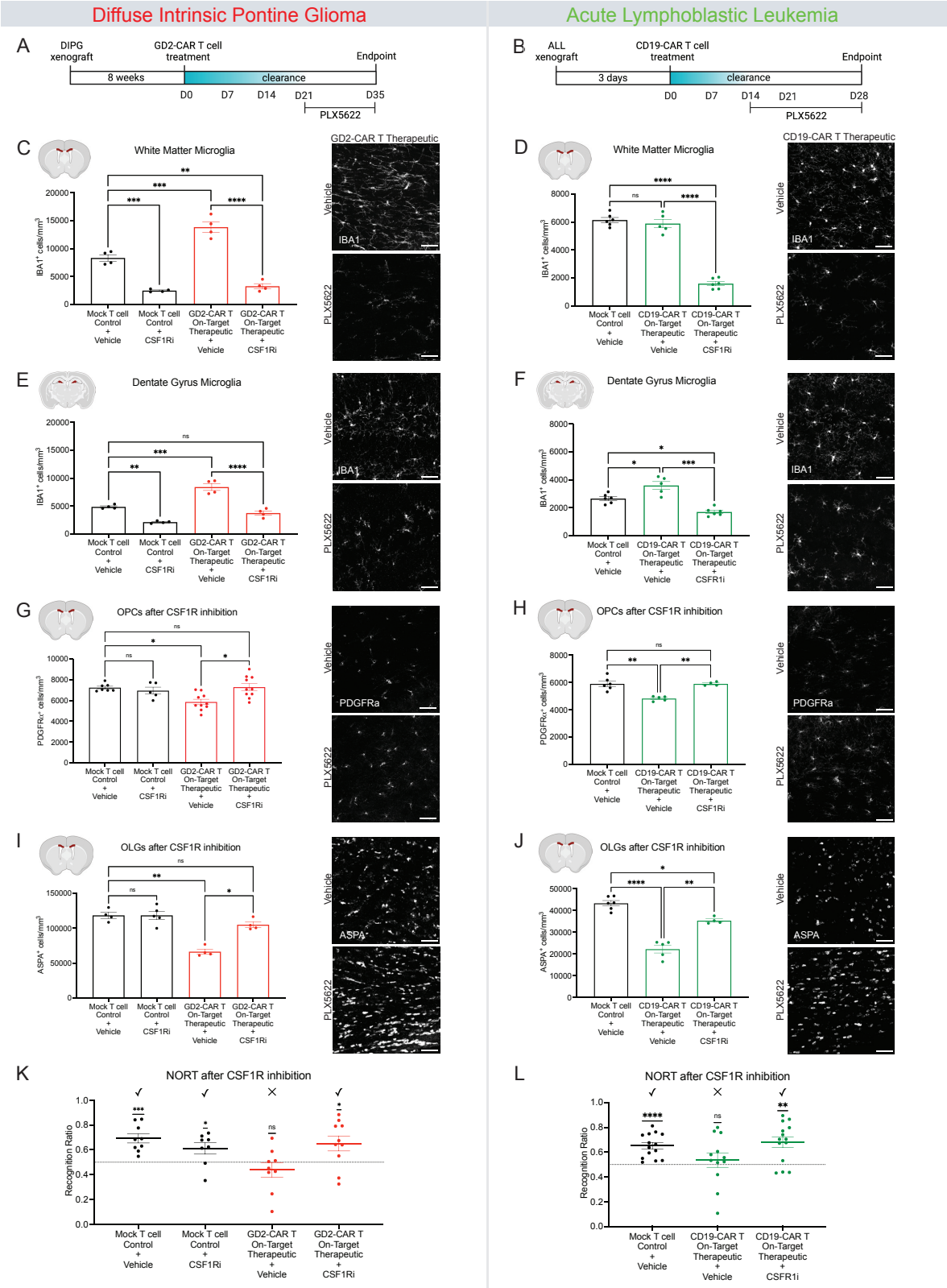
Figure 6. Microglial depletion rescues oligodendroglial dysregulation cognitive performance in novel object recognition testing

599 (A) Schematic illustrations of experimental timeline of the DIPG model including administration of
600 the CSF1R inhibitor (PLX5622).
601 (B) Schematic illustrations of experimental timeline of the ALL model including administration of
602 the CSF1R inhibitor (PLX5622).
603 (C) Quantification of DIPG xenografted mice corpus callosum white matter microglia (IBA1+) 35
604 days post-CAR T therapy with or without 14 days of CSF1R inhibition. Mock T cell+Vehicle Chow
605 (n=4 mice), mock T cell+CSF1Ri Chow (n=4 mice), GD2-CAR T Therapeutic+Vehicle Chow (n=4
606 mice), GD2-CAR T Therapeutic+CSF1Ri Chow (n=4 mice). Representative confocal micrographs
607 of microglia (white = IBA1) in the corpus callosum of DIPG xenografted mice 35 days after CAR
608 T cell therapy with or without 14 days of CSF1R inhibitor (PLX5622).
609 (D) Quantification of ALL xenografted mice corpus callosum white matter microglia (IBA1+) 28
610 days post-CAR T therapy with or without 14 days of CSF1R inhibition. Mock T cell+Vehicle Chow
611 (n=6 mice), CD19-CAR T Therapeutic+Vehicle Chow (n=5 mice), CD19-CAR T
612 Therapeutic+CSF1Ri Chow (n=6 mice). Representative confocal micrographs of microglia (white
613 = IBA1) in the corpus callosum of ALL xenografted mice 28 days after CAR T cell therapy with or
614 without 14 days of CSF1R inhibitor (PLX5622).
615 (E) Quantification of DIPG xenografted mice dentate gyrus microglia (IBA1+) 35 days post-CAR
616 T therapy with or without 14 days of CSF1R inhibition. Mock T cell+Vehicle Chow (n=4 mice),
617 mock T cell+CSF1Ri Chow (n=4 mice), GD2-CAR T Therapeutic+Vehicle Chow (n=4 mice), GD2-
618 CAR T Therapeutic+CSF1Ri Chow (n=4 mice). Representative confocal micrographs of microglia
619 (white = IBA1) in the dentate gyrus of DIPG xenografted mice 35 days after CAR T cell therapy
620 with or without 14 days of CSF1R inhibitor (PLX5622).
621 (F) Quantification of ALL xenografted mice dentate gyrus microglia (IBA1+) 28 days post-CAR T
622 therapy with or without 14 days of CSF1R inhibition. Mock T cell+Vehicle Chow (n=6 mice), CD19-
623 CAR T Therapeutic+Vehicle Chow (n=5), CD19-CAR T Therapeutic+CSF1Ri Chow (n=6 mice).
624 Representative confocal micrographs of microglia (white = IBA1) in the dentate gyrus of ALL
625 xenografted mice 28 days after CAR T cell therapy with or without 14 days of CSF1R inhibitor
626 (PLX5622).
627 (G) Quantification of DIPG xenografted mice oligodendrocyte precursor cells (PDGFRa+) 35 days
628 post-CAR T therapy with or without 14 days of CSF1R inhibition. Mock T cell+Vehicle Chow (n=7
629 mice), mock T cell+CSF1Ri Chow (n=5 mice), GD2-CAR T Therapeutic+Vehicle Chow (n=10
630 mice), GD2-CAR T Therapeutic+CSF1Ri Chow (n=10 mice). Representative confocal
631 micrographs of PDGFRa+ oligodendrocyte precursor cells (white = PDGFRa) in the corpus
632 callosum of DIPG xenografted mice 35 days after CAR T cell therapy with or without 14 days of
633 CSF1R inhibitor (PLX5622).
634 (H) Quantification of ALL xenografted mice oligodendrocyte precursor cells (PDGFRa+) 28 days
635 post-CAR T therapy with or without 14 days of CSF1R inhibition. Mock T cell+Vehicle Chow (n=6
636 mice), CD19-CAR T Therapeutic+Vehicle Chow (n=5 mice), CD19-CAR T Therapeutic+CSF1Ri
637 Chow (n=4 mice). Representative confocal micrographs of PDGFRa+ oligodendrocyte precursor
638 cells (white = PDGFRa) in the corpus callosum of ALL xenografted mice 28 days after CAR T cell
639 therapy with or without 14 days of CSF1R inhibitor (PLX5622).
640 (I) Quantification of DIPG xenografted mice mature oligodendrocytes (ASPA+) 35 days post-CAR
641 T therapy with or without 14 days of CSF1R inhibition. Mock T cell+Vehicle Chow (n=4 mice),
642 mock T cell+CSF1Ri Chow (n=5 mice), GD2-CAR T Therapeutic+Vehicle Chow (n=4 mice), GD2-
643 CAR T Therapeutic+CSF1Ri Chow (n=4 mice). Representative confocal micrographs of ASPA+
644 oligodendrocytes (white = ASPA) in the corpus callosum of DIPG xenografted mice 35 days after
645 CAR T cell therapy with or without 14 days of CSF1R inhibitor (PLX5622).
646 (J) Quantification of ALL xenografted mice mature oligodendrocytes (ASPA+) 28 days post-CAR
647 T therapy with or without 14 days of CSF1R inhibition. Mock T cell+Vehicle Chow (n=6 mice),
648 CD19-CAR T Therapeutic+Vehicle Chow (n=5 mice), CD19-CAR T Therapeutic+CSF1Ri Chow
649 (n=4 mice). Representative confocal micrographs of ASPA+ oligodendrocytes (white = ASPA) in

650 the corpus callosum of ALL xenografted mice 28 days after CAR T cell therapy with or without 14
651 days of CSF1R inhibitor (PLX5622).
652 (K) NORT results from DIPG xenografted mice 34 days post-CAR T therapy with or without 14
653 days of CSF1R inhibition. Mock T cell+Vehicle Chow (n=9 mice), mock T cell+CSF1Ri Chow (n=8
654 mice), GD2-CAR T Therapeutic+Vehicle Chow (n=9 mice), GD2-CAR T Therapeutic+CSF1Ri
655 Chow (n=10 mice).
656 (L) NORT results from ALL xenografted mice 27 days post-CAR T therapy with or without 14 days
657 of CSF1R inhibition. Mock T cell+Vehicle Chow (n=14 mice), CD19-CAR T Therapeutic+Vehicle
658 Chow (n=12 mice), CD19-CAR T Therapeutic+CSF1Ri Chow (n=14 mice).
659
660 Data shown as mean ± SEM (C-J). Each point = one mouse. ns = p > 0.05, * p < 0.05, **p < 0.01,
661 ***p < 0.001, ****p < 0.0001, analyzed via 2-way ANOVA.
662 (K and L) Data shown as mean ± SEM. Each point = one mouse. ns = p > 0.05, *p < 0.05, **p <
663 0.01, ***p < 0.001, ****p < 0.0001. Analyzed via One Sample T and Wilcoxon Test. Scale bars
664 equal 50um in all confocal images (A-J).
665
666
667
668
669
670
671
672
673
674
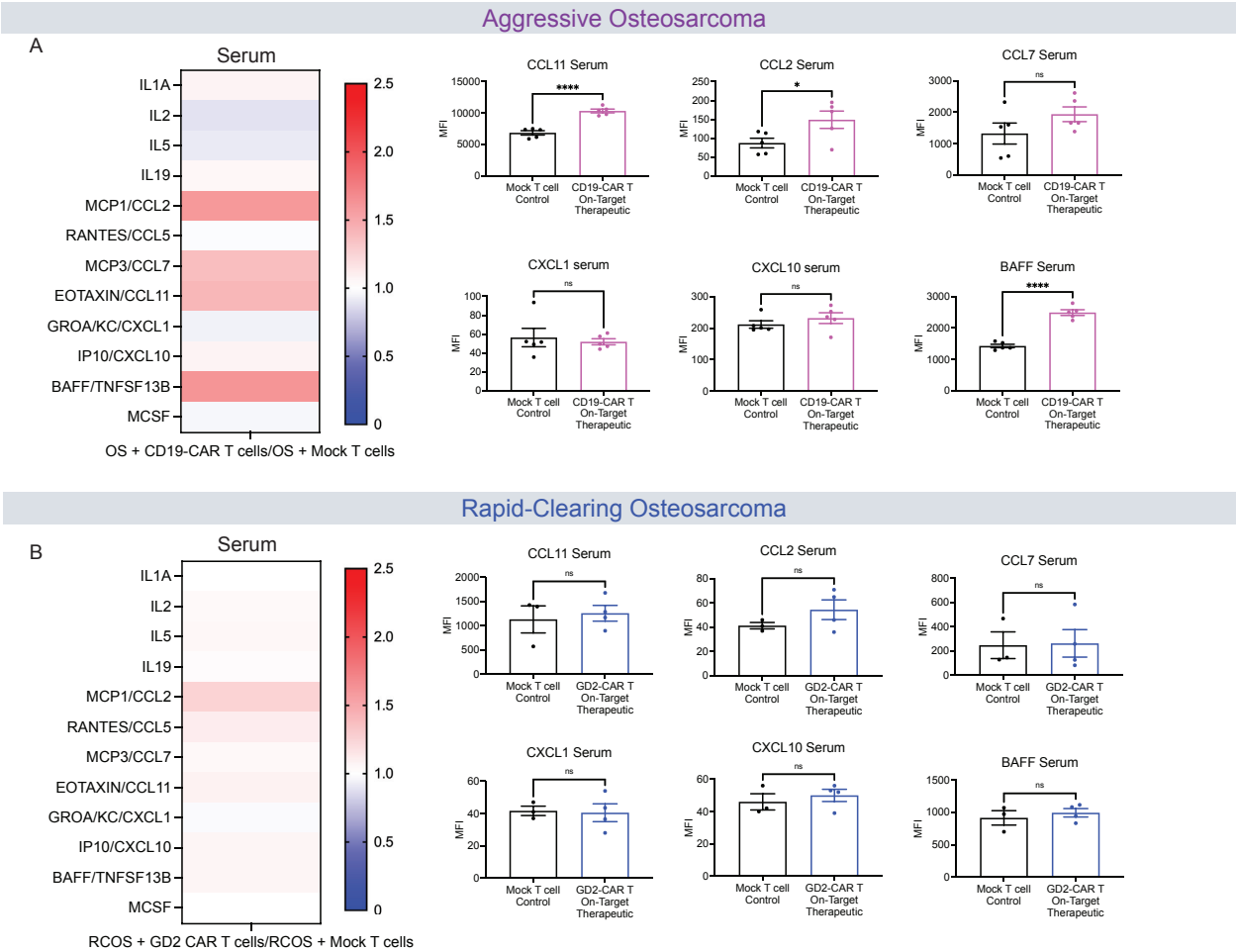
Supplemental Figure 1: Cytokine/chemokine measurements in the serum in two Osteosarcoma models

(A) Left, heat map of fold change of cytokine and chemokine analysis of serum in aggressive osteosarcoma (OS)+On-Target Therapeutic CD19-CAR T cell treated mice relative to aggressive osteosarcoma (OS)+mock T cell treated control mice 35-days post-CAR T cell therapy. Right, quantification of raw MFI of serum levels of cytokines (CCL11, CCL2, CCL7, CXCL1, CXCL10, BAFF).

(B) Left, heat map of fold change of cytokine and chemokine analysis of serum in rapid-clearing osteosarcoma (RCOS)+On-Target Therapeutic GD2-CAR T cell treated mice relative to rapid-clearing osteosarcoma (RCOS)+mock T cell treated control mice 35-days post-CAR T cell therapy. Right, quantification of raw MFI of serum levels of cytokines (CCL11, CCL2, CCL7, CXCL1, CXCL10, BAFF).

(A and B) Cytokine and chemokines significantly elevated or depressed, analyzed via Student's T test of raw MFI values.
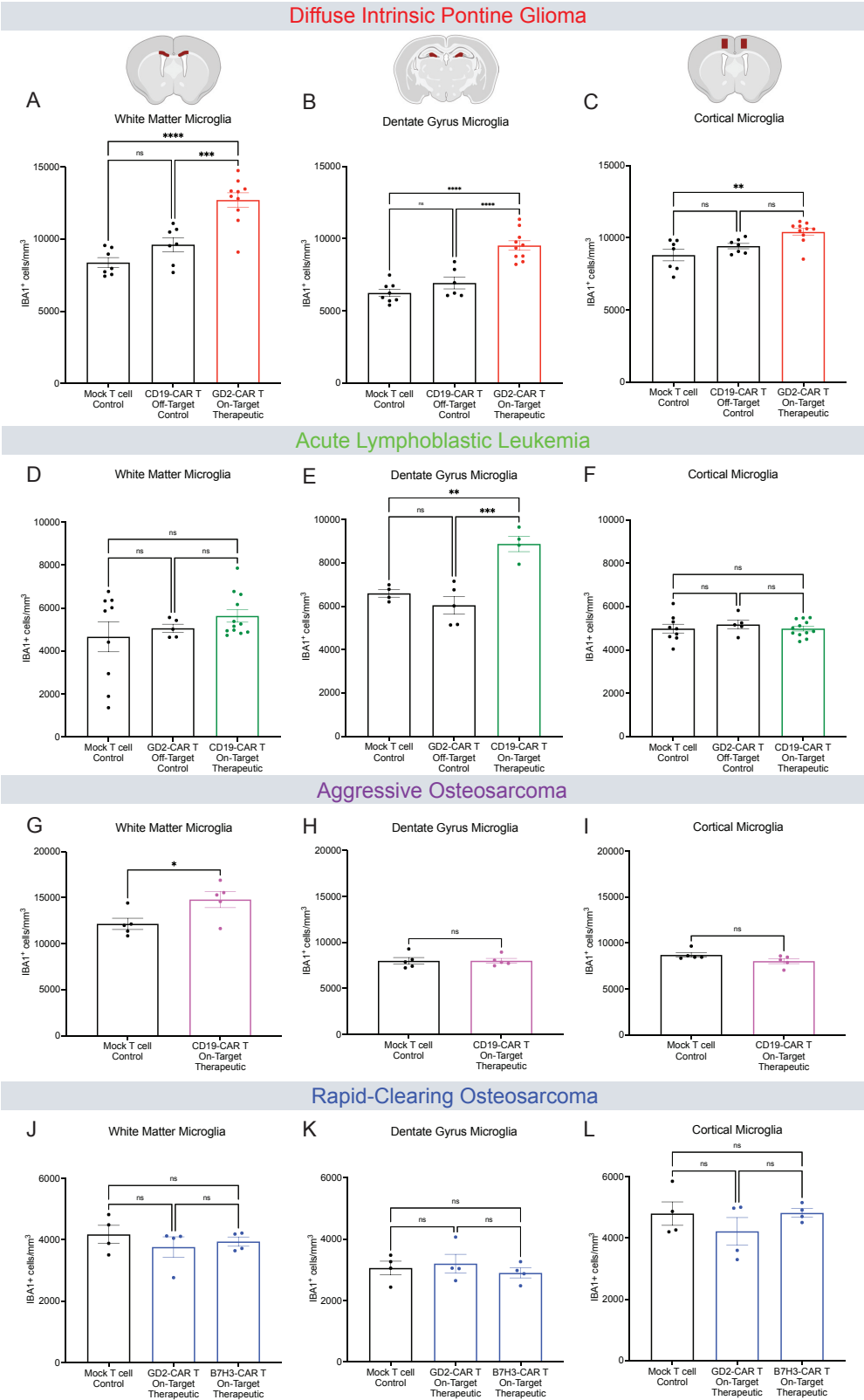
Supplemental Figure 2. Microglial density in the white matter, dentate gyrus, and cortex

694 (A) Microglia (IBA1+) quantification in the corpus callosum white matter 35 days post-CAR T
695 therapy in the DIPG model. Mock T cell Control (n=7 mice), CD19-CAR T Control (n=7 mice),
696 GD2-CAR T Therapeutic (n=10 mice).
697 (B) Microglia (IBA1+) quantification in the hilar white matter region of the dentate gyrus 35 days
698 post-CAR T therapy in the DIPG model. Mock T cell Control (n=8 mice), CD19-CAR T Control
699 (n=6 mice), GD2-CAR T Therapeutic (n=10 mice).
700 (C) Microglia (IBA1+) quantification in the cortical gray matter 35 days post-CAR T therapy in the
701 DIPG model. Mock T cell Control (n=7 mice), CD19-CAR T Control (n=7 mice), GD2-CAR T
702 Therapeutic (n=10 mice).
703 (D) Microglia (IBA1+) quantification in the corpus callosum white matter 35 days post-CAR T
704 therapy in the ALL model. Mock T cell Control (n=9 mice), GD2-CAR T Control (n=5 mice), CD19-
705 CAR T Therapeutic (n=12 mice).
706 (E) Microglia (IBA1+) quantification in the hilar white matter region of the dentate gyrus 35 days
707 post-CAR T therapy in the ALL model. Mock T cell Control (n=4 mice), GD2-CAR T Control (n=5
708 mice), CD19-CAR T Therapeutic (n=4 mice).
709 (F) Microglia (IBA1+) quantification in the cortical gray matter 35 days post-CAR T therapy in the
710 ALL model. Mock T cell Control (n=9 mice), GD2-CAR T Control (n=5 mice), CD19-CAR T
711 Therapeutic (n=12 mice).
712 (G) Microglia (IBA1+) quantification in the corpus callosum white matter 35 days post-CAR T
713 therapy in the aggressive osteosarcoma model. Mock T cell Control (n=5 mice), CD19-CAR T
714 Therapeutic (n=5 mice).
715 (H) Microglia (IBA1+) quantification in the hilar white matter region of the dentate gyrus 35 days
716 post-CAR T therapy in the aggressive osteosarcoma model. Mock T cell Control (n=5 mice),
717 CD19-CAR T Therapeutic (n=5 mice).
718 (I) Microglia (IBA1+) quantification in the cortical gray matter 35 days post-CAR T therapy in the
719 aggressive osteosarcoma model. Mock T cell Control (n=5 mice), CD19-CAR T Therapeutic (n=5
720 mice).
721 (J) Microglia (IBA1+) quantification in the corpus callosum white matter 35 days post-CAR T
722 therapy in the rapid-clearing osteosarcoma model. Mock T cell Control (n=4 mice), GD2-CAR T
723 Therapeutic (n=4 mice), B7H3-CAR T Therapeutic (n=4 mice).
724 (K) Microglia (IBA1+) quantification in the hilar white matter region of the dentate gyrus 35 days
725 post-CAR T therapy in the rapid-clearing osteosarcoma model. Mock T cell Control (n=4 mice),
726 GD2-CAR T Therapeutic (n=4 mice), B7H3-CAR T Therapeutic (n=4 mice).
727 (L) Microglia (IBA1+) quantification in the cortical gray matter 35 days post-CAR T therapy in the
728 rapid-clearing osteosarcoma model. Mock T cell Control (n=4 mice), GD2-CAR T Therapeutic
729 (n=4 mice), B7H3-CAR T Therapeutic (n=4 mice).
730
731 Data shown as mean ± SEM (A-F, J-L). Each point = one mouse. ns = $p > 0.05$, *$p < 0.05$, **$p <$
732 0.01, ***$p < 0.001$, ****$p < 0.0001$, analyzed via One-way ANOVA.
733 (G-I) Data shown as mean ± SEM. Each point = one mouse, ns = $p > 0.05$, *$p < 0.05$, analyzed
734 via Unpaired T Test.
735
736
737
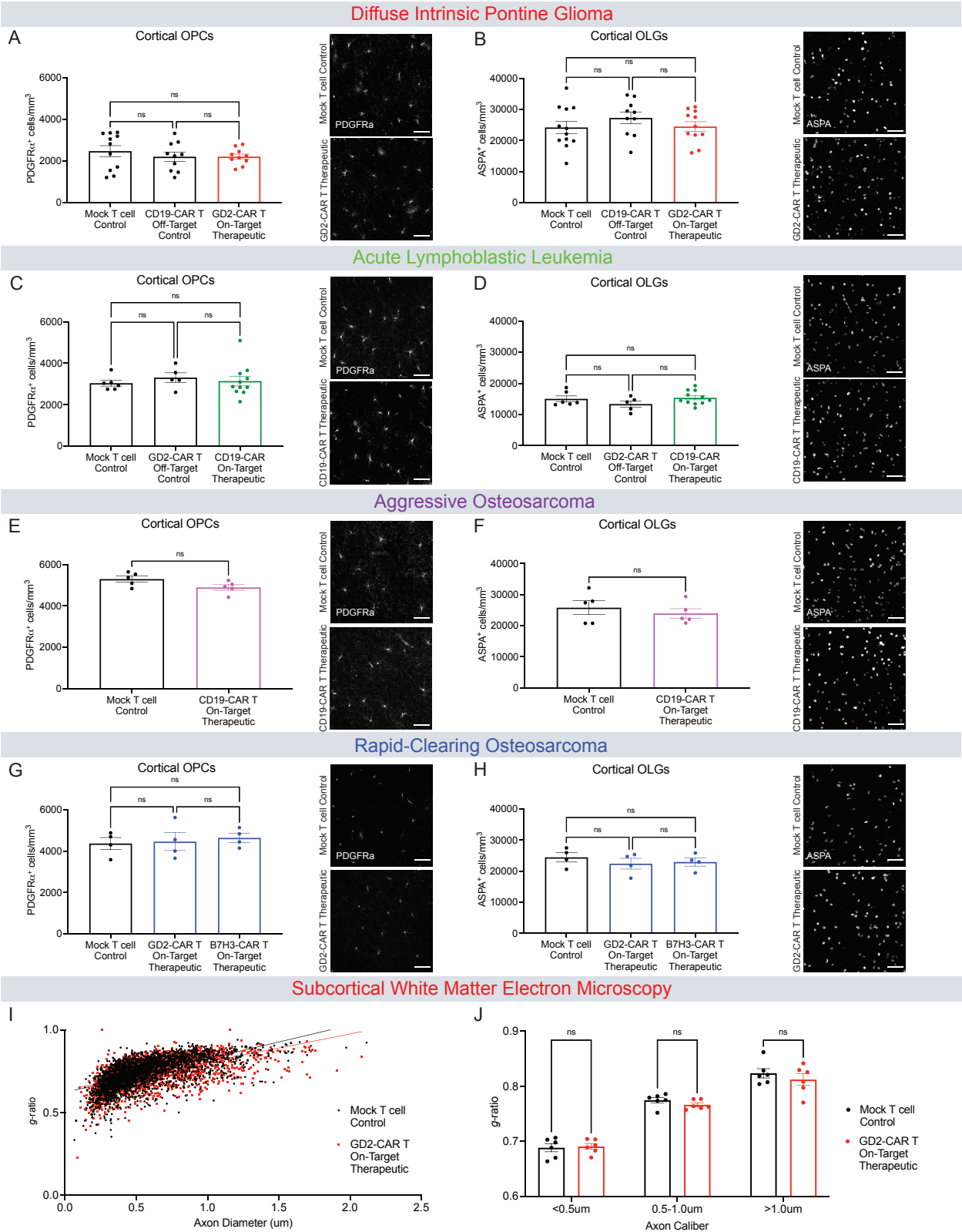
Supplemental Figure 3. Normal cortical oligodendroglia and subcortical myelin sheath thickness following tumor-clearing CAR T cell therapy

(A) Quantification and representative confocal micrographs of PDGFRa+ oligodendrocyte precursor cells from the cortical gray matter in DIPG xenografted mice 35 days post-CAR T therapy. Mock T cell Control (n=11 mice), CD19-CAR T Control (n=10 mice), GD2-CAR T Therapeutic (n=10 mice).

(B) Quantification and representative confocal micrographs of ASPA+ mature oligodendrocytes from the cortical gray matter in DIPG xenografted mice 35 days post-CAR T therapy. Mock T cell Control (n=12 mice), CD19-CAR T Control (n=10 mice), GD2-CAR T Therapeutic (n=11 mice).

(C) Quantification and representative confocal micrographs of PDGFRa+ oligodendrocyte precursor cells from the cortical gray matter in ALL xenografted mice 28 days post-CAR T therapy. Mock T cell Control (n=6 mice), GD2-CAR T Control (n=5 mice), CD19-CAR T Therapeutic (n=11 mice).

(D) Quantification and representative confocal micrographs of ASPA+ mature oligodendrocytes from the cortical gray matter in ALL xenografted mice 28 days post-CAR T therapy. Mock T cell Control (n=6 mice), CD19-CAR T Control (n=5 mice), GD2-CAR T Therapeutic (n=10 mice).

(E) Quantification and representative confocal micrographs of PDGFRa+ oligodendrocyte precursor cells from the cortical gray matter in aggressive osteosarcoma xenografted mice 35 days post-CAR T therapy. Mock T cell Control (n=5 mice), CD19-CAR T Therapeutic (n=5 mice).

(F) Quantification and representative confocal micrographs of ASPA+ mature oligodendrocytes from the cortical gray matter in aggressive osteosarcoma xenografted mice 35 days post-CAR T therapy. Mock T cell Control (n=5 mice), CD19-CAR T Therapeutic (n=5 mice).

(G) Quantification and representative confocal micrographs of PDGFRa+ oligodendrocyte precursor cells from the cortical gray matter in rapid-clearing osteosarcoma xenografted mice 35 days post-CAR T therapy. Mock T cell Control (n=4 mice), GD2-CAR T Therapeutic l (n=4 mice), B7H3-CAR T Therapeutic (n=4 mice).

(H) Quantification and representative confocal micrographs of ASPA+ mature oligodendrocytes from the cortical gray matter in rapid-clearing osteosarcoma xenografted mice 35 days post-CAR T therapy. Mock T cell Control (n=4 mice), GD2-CAR T Therapeutic l (n=4 mice), B7H3-CAR T Therapeutic (n=4 mice).

(I) Scatterplots of g-ratio relative to axon diameter at 35 days post-CAR T cell therapy for mock T cell control (black points) or GD2-CAR T On-Target Therapeutic (red points) treated mice. (n=6 mice per group)

(J) G-ratio relative to small (<0.5um), medium (0.5-1.0um), and large (>1.0um) caliber axons for mock T cell control (black points) or GD2-CAR T On-Target Therapeutic (red points) treated mice. (n=6 mice per group)

(A-D, G-H, J) Data shown as mean ± SEM. Each point = one mouse. ns = $p > 0.05$, analyzed via One-way ANOVA.

(E & F) Data shown as mean ± SEM. Each point = one mouse, ns = $p > 0.05$, analyzed via Unpaired T Test. Scale bars equal 50um in all confocal images.
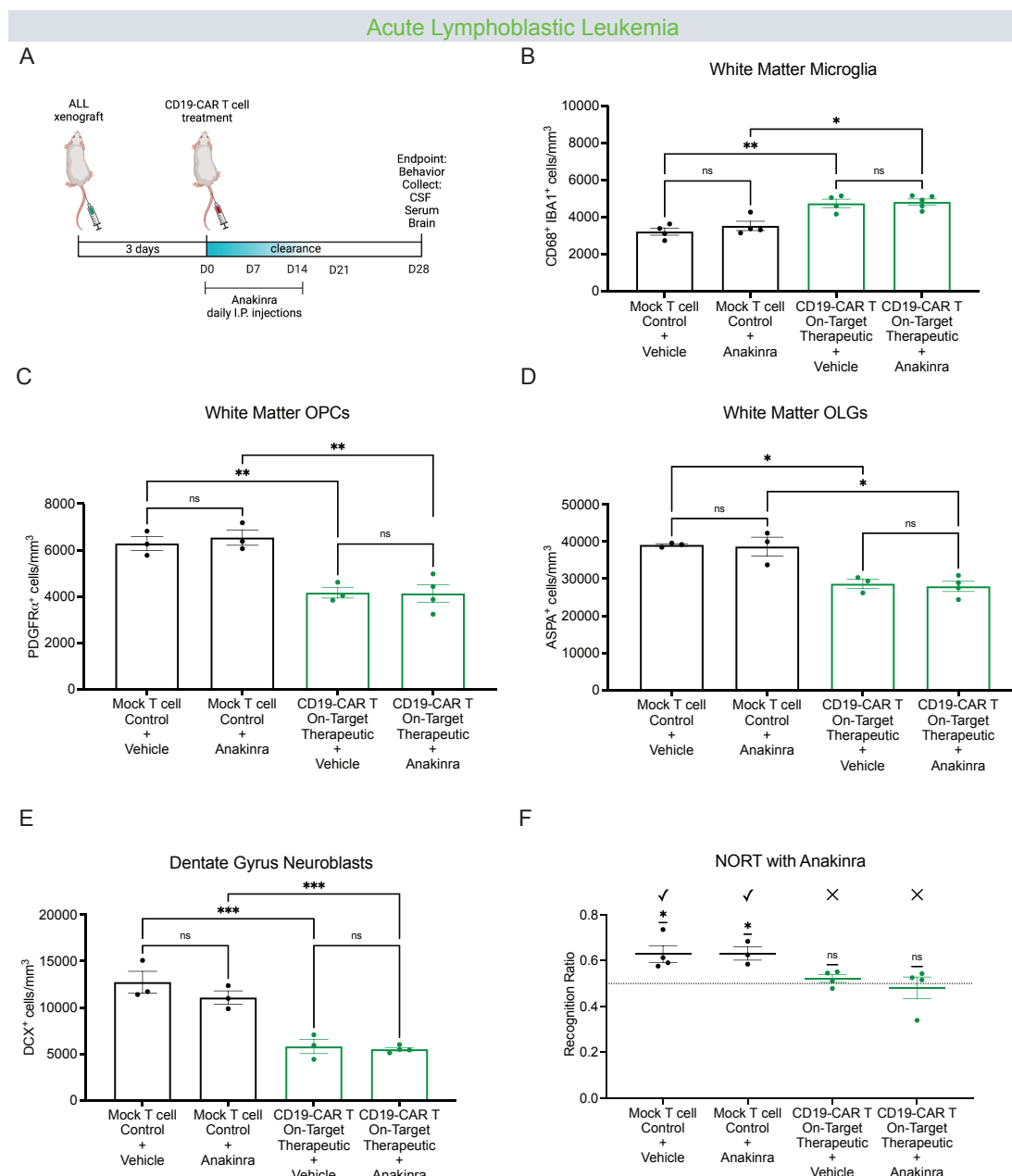
Supplemental Figure 4. Anakinra does not rescue cellular or behavioral deficits

(A) Schematic illustration denoting the timeline for the ALL model with Anakinra administration.
(B) Quantification of corpus callosum reactive white matter microglia (IBA1+ CD68+) 28 days post-CAR T therapy with or without 14 days of Anakinra administration in ALL-xenografted mice. Mock T cell+Vehicle (n=4 mice), mock T cell+Anakinra (n=4 mice), CD19-CAR T Therapeutic+Vehicle (n=4 mice), CD19-CAR T Therapeutic+Anakinra (n=5 mice).
(C) Quantification of PDGFRa+ oligodendrocyte precursor cells from the corpus callosum in ALL-xenografted mice 28 days post-CAR T therapy with or without 14 days of Anakinra administration. Mock T cell+Vehicle (n=4 mice), mock T cell+Anakinra (n=4 mice), CD19-CAR T Therapeutic+Vehicle (n=4 mice), CD19-CAR T Therapeutic+Anakinra (n=5 mice).
(D) Quantification of ASPA+ mature oligodendrocytes from the corpus callosum in ALL-xenografted mice 28 days 28 days post-CAR T therapy with or without 14 days of Anakinra

797   administration. Mock T cell+Vehicle (n=4 mice), mock T cell+Anakinra (n=4 mice), CD19-CAR T
798   Therapeutic+Vehicle (n=4 mice), CD19-CAR T Therapeutic+Anakinra (n=5 mice).

799   (E) Quantification of dentate gyrus neuroblasts (DCX+) 28 days post-CAR T therapy with or
800   without 14 days of Anakinra administration in ALL-xenografted mice. Mock T cell+Vehicle (n=3
801   mice), mock T cell+Anakinra (n=3 mice), CD19-CAR T Therapeutic+Vehicle (n=3 mice), CD19-
802   CAR T Therapeutic+Anakinra (n=4 mice).

803   (F) NORT performed for ALL-xenografted mice analyzed on day 28 post-CAR T therapy with or
804   without Anakinra administration. Mock T cell+Vehicle (n=4 mice), mock T cell+Anakinra (n=3
805   mice), CD19-CAR T Therapeutic+Vehicle (n=4 mice), CD19-CAR T Therapeutic+Anakinra (n=4
806   mice).

807

808   (B, C, D, E) Data shown as mean ± SEM. Each point = one mouse. ns = $p > 0.05$, **$p < 0.01$, ***p
809   < 0.001, analyzed via 2-way ANOVA.

810   (F) Data shown as mean ± SEM. Each point = one mouse. ns = $p > 0.05$, *$p < 0.05$, **$p < 0.01$,
811   ****$p < 0.0001$. Analyzed via One Sample T and Wilcoxon Test.

812

813

814

815

816

817

818

819
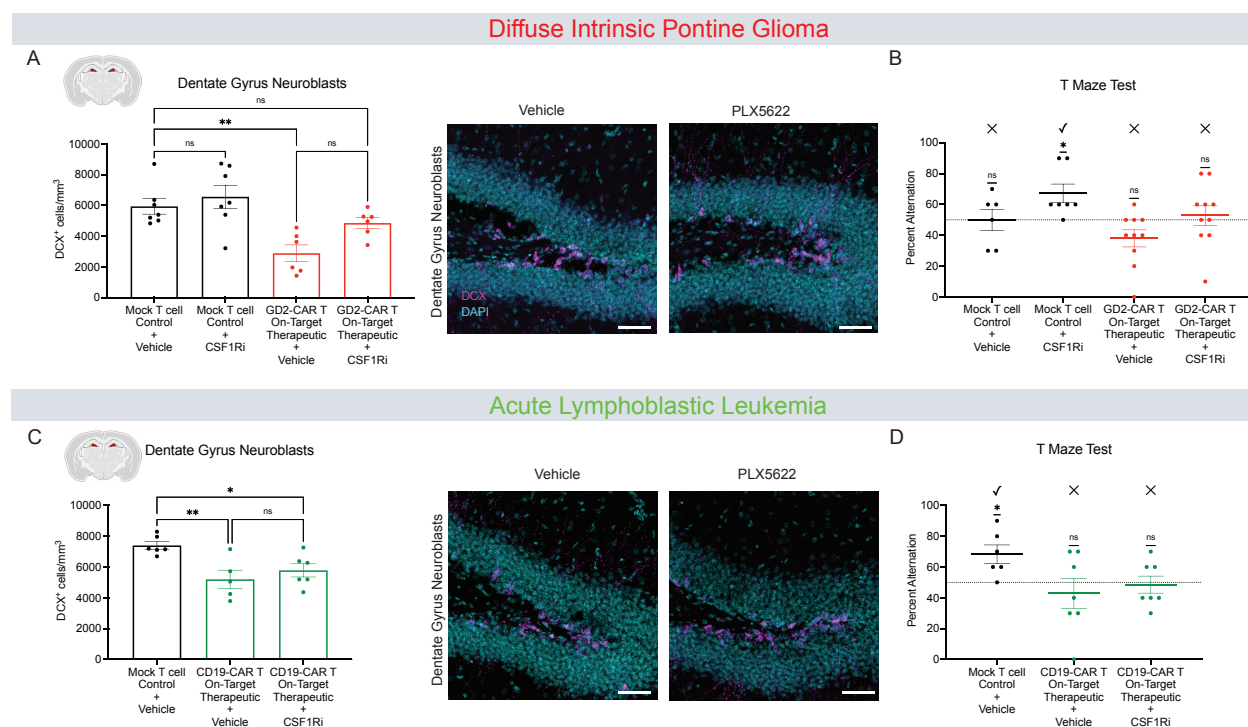
Supplemental Figure 5. Incomplete microglial depletion in the hippocampus does not rescue behavioral deficits

(A) Quantification of dentate gyrus neuroblasts (DCX+) 35 days post-CAR T therapy with or without 14 days of CSF1R inhibition in DIPG-xenografted mice,. Mock T cell+Vehicle Chow (n=7 mice), mock T cell+CSF1Ri Chow (n=7 mice), GD2-CAR T Therapeutic+Vehicle Chow (n=6 mice), GD2-CAR T Therapeutic+CSF1Ri Chow (n=6 mice). Representative confocal micrographs of neuroblasts (magenta = DCX, cyan = DAPI) in the dentate gyrus of DIPG xenografted mice 35 days after CAR T cell therapy with or without 14 days of CSF1R inhibitor (PLX5622).

(B) T Maze Test results from DIPG-xenografted mice D35 post-CAR T therapy with or without 14 days of CSF1R inhibition. Mock T cell+Vehicle Chow (n=6 mice), mock T cell+CSF1Ri Chow (n=7 mice), GD2-CAR T Therapeutic+Vehicle Chow (n=10 mice), GD2-CAR T Therapeutic+CSF1Ri Chow (n=10 mice).

(C) Quantification of dentate gyrus neuroblasts (DCX+) in ALL-xenografted mice at 28 days post-CAR T therapy with or without 14 days of CSF1R inhibition. Mock T cell+Vehicle Chow (n=6 mice), CD19-CAR T Therapeutic+Vehicle Chow (n=5 mice), CD19-CAR T Therapeutic+CSF1Ri Chow (n=6 mice). Representative confocal micrographs of neuroblasts (magenta = DCX, cyan = DAPI) in the dentate gyrus of ALL xenografted mice 28 days after CAR T cell therapy with or without 14 days of CSF1R inhibitor (PLX5622).

(D) T maze Test results from ALL-xenografted mice at D28 post-CAR T therapy with or without 14 days of CSF1R inhibition. Mock T cell+Vehicle Chow (n=6 mice), CD19-CAR T Therapeutic+Vehicle Chow (n=7 mice), CD19-CAR T Therapeutic+CSF1Ri Chow (n=7 mice).

Data shown as mean ± SEM (A-D). Each point = one mouse. ns = $p > 0.05$, * $p < 0.05$, **$p < 0.01$, analyzed via 2-way ANOVA (A, C), One Sample T and Wilcoxon Test (B, D). Scale bars equal 50um in all confocal images.

References Cited

1. Wefel, J.S., Kesler, S.R., Noll, K.R., and Schagen, S.B. (2015). Clinical characteristics, pathophysiology, and management of noncentral nervous system cancer-related cognitive impairment in adults. CA Cancer J Clin *65*, 123-138. 10.3322/caac.21258.

2. Mabbott, D.J., Spiegler, B.J., Greenberg, M.L., Rutka, J.T., Hyder, D.J., and Bouffet, E. (2005). Serial evaluation of academic and behavioral outcome after treatment with cranial radiation in childhood. J Clin Oncol *23*, 2256-2263. 10.1200/JCO.2005.01.158.

3. Ruark, J., Mullane, E., Cleary, N., Cordeiro, A., Bezerra, E.D., Wu, V., Voutsinas, J., Shaw, B.E., Flynn, K.E., Lee, S.J., et al. (2020). Patient-Reported Neuropsychiatric Outcomes of Long-Term Survivors after Chimeric Antigen Receptor T Cell Therapy. Biol Blood Marrow Transplant *26*, 34-43. 10.1016/j.bbmt.2019.09.037.

4. Barata, A., Hoogland, A.I., Kommalapati, A., Logue, J., Welniak, T., Hyland, K.A., Eisel, S.L., Small, B.J., Jayani, R.V., Booth-Jones, M., et al. (2022). Change in Patients' Perceived Cognition Following Chimeric Antigen Receptor T-Cell Therapy for Lymphoma. Transplant Cell Ther *28*, 401.e401-401.e407. 10.1016/j.jtct.2022.05.015.

5. Rogiers, A., Boekhout, A., Schwarze, J.K., Awada, G., Blank, C.U., and Neyns, B. (2019). Long-Term Survival, Quality of Life, and Psychosocial Outcomes in Advanced Melanoma Patients Treated with Immune Checkpoint Inhibitors. J Oncol *2019*, 5269062. 10.1155/2019/5269062.

6. Schagen, S.B., Tsvetkov, A.S., Compter, A., and Wefel, J.S. (2022). Cognitive adverse effects of chemotherapy and immunotherapy: are interventions within reach? Nat Rev Neurol *18*, 173-185. 10.1038/s41582-021-00617-2.

7. Monje, M.L., Mizumatsu, S., Fike, J.R., and Palmer, T.D. (2002). Irradiation induces neural precursor-cell dysfunction. Nat Med *8*, 955-962. 10.1038/nm749.

8. Monje, M.L., Toda, H., and Palmer, T.D. (2003). Inflammatory blockade restores adult hippocampal neurogenesis. Science *302*, 1760-1765. 10.1126/science.1088417.

9. Monje, M.L., Vogel, H., Masek, M., Ligon, K.L., Fisher, P.G., and Palmer, T.D. (2007). Impaired human hippocampal neurogenesis after treatment for central nervous system malignancies. Ann Neurol *62*, 515-520. 10.1002/ana.21214.

10. Li, M.D., Burns, T.C., Kumar, S., Morgan, A.A., Sloan, S.A., and Palmer, T.D. (2015). Aging-like changes in the transcriptome of irradiated microglia. Glia *63*, 754-767. 10.1002/glia.22782.

11. Gibson, E.M., Nagaraja, S., Ocampo, A., Tam, L.T., Wood, L.S., Pallegar, P.N., Greene, J.J., Geraghty, A.C., Goldstein, A.K., Ni, L., et al. (2019). Methotrexate Chemotherapy Induces Persistent Tri-glial Dysregulation that Underlies Chemotherapy-Related Cognitive Impairment. Cell *176*, 43-55.e13. 10.1016/j.cell.2018.10.049.

12. Geraghty, A.C., Gibson, E.M., Ghanem, R.A., Greene, J.J., Ocampo, A., Goldstein, A.K., Ni, L., Yang, T., Marton, R.M., Paşca, S.P., et al. (2019). Loss of Adaptive Myelination Contributes to Methotrexate Chemotherapy-Related Cognitive Impairment. Neuron *103*, 250-265.e258. 10.1016/j.neuron.2019.04.032.

13. Seigers, R., Timmermans, J., van der Horn, H.J., de Vries, E.F., Dierckx, R.A., Visser, L., Schagen, S.B., van Dam, F.S., Koolhaas, J.M., and Buwalda, B. (2010). Methotrexate reduces hippocampal blood vessel density and activates microglia in rats but does not

892   elevate central cytokine release. Behav Brain Res *207*, 265-272.
893   10.1016/j.bbr.2009.10.009.

894 14.   Hammond, T.R., Dufort, C., Dissing-Olesen, L., Giera, S., Young, A., Wysoker, A., Walker,
895   A.J., Gergits, F., Segel, M., Nemesh, J., et al. (2019). Single-Cell RNA Sequencing of
896   Microglia throughout the Mouse Lifespan and in the Injured Brain Reveals Complex Cell-
897   State Changes. Immunity *50*, 253-271.e256. 10.1016/j.immuni.2018.11.004.

898 15.   Fernández-Castañeda, A., Lu, P., Geraghty, A.C., Song, E., Lee, M.H., Wood, J., O'Dea, M.R.,
899   Dutton, S., Shamardani, K., Nwangwu, K., et al. (2022). Mild respiratory COVID can cause
900   multi-lineage neural cell and myelin dysregulation. Cell *185*, 2452-2468.e2416.
901   10.1016/j.cell.2022.06.008.

902 16.   Liddelow, S.A., Guttenplan, K.A., Clarke, L.E., Bennett, F.C., Bohlen, C.J., Schirmer, L.,
903   Bennett, M.L., Münch, A.E., Chung, W.S., Peterson, T.C., et al. (2017). Neurotoxic reactive
904   astrocytes are induced by activated microglia. Nature *541*, 481-487.
905   10.1038/nature21029.

906 17.   Gibson, E.M., and Monje, M. (2021). Microglia in Cancer Therapy-Related Cognitive
907   Impairment. Trends Neurosci *44*, 441-451. 10.1016/j.tins.2021.02.003.

908 18.   Sengsayadeth, S., Savani, B.N., Oluwole, O., and Dholaria, B. (2022). Overview of approved
909   CAR-T therapies, ongoing clinical trials, and its impact on clinical practice. EJHaem *3*, 6-
910   10. 10.1002/jha2.338.

911 19.   Mount, C.W., Majzner, R.G., Sundaresh, S., Arnold, E.P., Kadapakkam, M., Haile, S.,
912   Labanieh, L., Hulleman, E., Woo, P.J., Rietberg, S.P., et al. (2018). Potent antitumor
913   efficacy of anti-GD2 CAR T cells in H3-K27M. Nat Med *24*, 572-579. 10.1038/s41591-018-
914   0006-x.

915 20.   Majzner, R.G., Ramakrishna, S., Yeom, K.W., Patel, S., Chinnasamy, H., Schultz, L.M.,
916   Richards, R.M., Jiang, L., Barsan, V., Mancusi, R., et al. (2022). GD2-CAR T cell therapy for
917   H3K27M-mutated diffuse midline gliomas. Nature *603*, 934-941. 10.1038/s41586-022-
918   04489-4.

919 21.   Holtzman, N.G., Xie, H., Bentzen, S., Kesari, V., Bukhari, A., El Chaer, F., Lutfi, F., Siglin, J.,
920   Hutnick, E., Gahres, N., et al. (2021). Immune effector cell-associated neurotoxicity
921   syndrome after chimeric antigen receptor T-cell therapy for lymphoma: predictive
922   biomarkers and clinical outcomes. Neuro Oncol *23*, 112-121. 10.1093/neuonc/noaa183.

923 22.   Lee, D.W., Santomasso, B.D., Locke, F.L., Ghobadi, A., Turtle, C.J., Brudno, J.N., Maus,
924   M.V., Park, J.H., Mead, E., Pavletic, S., et al. (2019). ASTCT Consensus Grading for Cytokine
925   Release Syndrome and Neurologic Toxicity Associated with Immune Effector Cells. Biol
926   Blood Marrow Transplant *25*, 625-638. 10.1016/j.bbmt.2018.12.758.

927 23.   Ren, L., Mendoza, A., Zhu, J., Briggs, J.W., Halsey, C., Hong, E.S., Burkett, S.S., Morrow, J.,
928   Lizardo, M.M., Osborne, T., et al. (2015). Characterization of the metastatic phenotype of
929   a panel of established osteosarcoma cells. Oncotarget *6*, 29469-29481.
930   10.18632/oncotarget.5177.

931 24.   Long, A.H., Haso, W.M., Shern, J.F., Wanhainen, K.M., Murgai, M., Ingaramo, M., Smith,
932   J.P., Walker, A.J., Kohler, M.E., Venkateshwara, V.R., et al. (2015). 4-1BB costimulation
933   ameliorates T cell exhaustion induced by tonic signaling of chimeric antigen receptors.
934   Nat Med *21*, 581-590. 10.1038/nm.3838.

935   25.   Majzner, R.G., Rietberg, S.P., Sotillo, E., Dong, R., Vachharajani, V.T., Labanieh, L.,
936   Myklebust, J.H., Kadapakkam, M., Weber, E.W., Tousley, A.M., et al. (2020). Tuning the
937   Antigen Density Requirement for CAR T-cell Activity. Cancer Discov *10*, 702-723.
938   10.1158/2159-8290.CD-19-0945.
939   26.   Majzner, R.G., Theruvath, J.L., Nellan, A., Heitzeneder, S., Cui, Y., Mount, C.W., Rietberg,
940   S.P., Linde, M.H., Xu, P., Rota, C., et al. (2019). CAR T Cells Targeting B7-H3, a Pan-Cancer
941   Antigen, Demonstrate Potent Preclinical Activity Against Pediatric Solid Tumors and Brain
942   Tumors. Clin Cancer Res *25*, 2560-2574. 10.1158/1078-0432.CCR-18-0432.
943   27.   d'Isa, R., Comi, G., and Leocani, L. (2021). Apparatus design and behavioural testing
944   protocol for the evaluation of spatial working memory in mice through the spontaneous
945   alternation T-maze. Sci Rep *11*, 21177. 10.1038/s41598-021-00402-7.
946   28.   Deacon, R.M., and Rawlins, J.N. (2006). T-maze alternation in the rodent. Nat Protoc *1*, 7-
947   12. 10.1038/nprot.2006.2.
948   29.   Villeda, S.A., Luo, J., Mosher, K.I., Zou, B., Britschgi, M., Bieri, G., Stan, T.M., Fainberg, N.,
949   Ding, Z., Eggel, A., et al. (2011). The ageing systemic milieu negatively regulates
950   neurogenesis and cognitive function. Nature *477*, 90-94. 10.1038/nature10357.
951   30.   Vallières, L., Campbell, I.L., Gage, F.H., and Sawchenko, P.E. (2002). Reduced hippocampal
952   neurogenesis in adult transgenic mice with chronic astrocytic production of interleukin-6.
953   J Neurosci *22*, 486-492. 10.1523/JNEUROSCI.22-02-00486.2002.
954   31.   Drapeau, E., Mayo, W., Aurousseau, C., Le Moal, M., Piazza, P.V., and Abrous, D.N. (2003).
955   Spatial memory performances of aged rats in the water maze predict levels of
956   hippocampal neurogenesis. Proc Natl Acad Sci U S A *100*, 14385-14390.
957   10.1073/pnas.2334169100.
958   32.   Driscoll, I., Howard, S.R., Stone, J.C., Monfils, M.H., Tomanek, B., Brooks, W.M., and
959   Sutherland, R.J. (2006). The aging hippocampus: a multi-level analysis in the rat.
960   Neuroscience *139*, 1173-1185. 10.1016/j.neuroscience.2006.01.040.
961   33.   Madsen, T.M., Kristjansen, P.E., Bolwig, T.G., and Wörtwein, G. (2003). Arrested neuronal
962   proliferation and impaired hippocampal function following fractionated brain irradiation
963   in the adult rat. Neuroscience *119*, 635-642. 10.1016/s0306-4522(03)00199-4.
964   34.   Clelland, C.D., Choi, M., Romberg, C., Clemenson, G.D., Fragniere, A., Tyers, P., Jessberger,
965   S., Saksida, L.M., Barker, R.A., Gage, F.H., and Bussey, T.J. (2009). A functional role for
966   adult hippocampal neurogenesis in spatial pattern separation. Science *325*, 210-213.
967   10.1126/science.1173215.
968   35.   Rao, M.S., and Shetty, A.K. (2004). Efficacy of doublecortin as a marker to analyse the
969   absolute number and dendritic growth of newly generated neurons in the adult dentate
970   gyrus. Eur J Neurosci *19*, 234-246. 10.1111/j.0953-816x.2003.03123.x.
971   36.   Couillard-Despres, S., Winner, B., Schaubeck, S., Aigner, R., Vroemen, M., Weidner, N.,
972   Bogdahn, U., Winkler, J., Kuhn, H.G., and Aigner, L. (2005). Doublecortin expression levels
973   in adult brain reflect neurogenesis. Eur J Neurosci *21*, 1-14. 10.1111/j.1460-
974   9568.2004.03813.x.
975   37.   Wehrli, M., Gallagher, K., Chen, Y.B., Leick, M.B., McAfee, S.L., El-Jawahri, A.R., DeFilipp,
976   Z., Horick, N., O'Donnell, P., Spitzer, T., et al. (2022). Single-center experience using
977   anakinra for steroid-refractory immune effector cell-associated neurotoxicity syndrome
978   (ICANS). J Immunother Cancer *10*. 10.1136/jitc-2021-003847.

979   38.   Strati, P., Ahmed, S., Kebriaei, P., Nastoupil, L.J., Claussen, C.M., Watson, G., Horowitz, S.B., Brown, A.R.T., Do, B., Rodriguez, M.A., et al. (2020). Clinical efficacy of anakinra to mitigate CAR T-cell therapy-associated toxicity in large B-cell lymphoma. Blood Adv *4*, 3123-3127. 10.1182/bloodadvances.2020002328.

983   39.   Acharya, M.M., Green, K.N., Allen, B.D., Najafi, A.R., Syage, A., Minasyan, H., Le, M.T., Kawashita, T., Giedzinski, E., Parihar, V.K., et al. (2016). Elimination of microglia improves cognitive function following cranial irradiation. Sci Rep *6*, 31545. 10.1038/srep31545.

986   40.   Dagher, N.N., Najafi, A.R., Kayala, K.M., Elmore, M.R., White, T.E., Medeiros, R., West, B.L., and Green, K.N. (2015). Colony-stimulating factor 1 receptor inhibition prevents microglial plaque association and improves cognition in 3xTg-AD mice. J Neuroinflammation *12*, 139. 10.1186/s12974-015-0366-9.

990   41.   Elmore, M.R., Najafi, A.R., Koike, M.A., Dagher, N.N., Spangenberg, E.E., Rice, R.A., Kitazawa, M., Matusow, B., Nguyen, H., West, B.L., and Green, K.N. (2014). Colony-stimulating factor 1 receptor signaling is necessary for microglia viability, unmasking a microglia progenitor cell in the adult brain. Neuron *82*, 380-397. 10.1016/j.neuron.2014.02.040.

995   42.   Zhan, L., Fan, L., Kodama, L., Sohn, P.D., Wong, M.Y., Mousa, G.A., Zhou, Y., Li, Y., and Gan, L. (2020). A MAC2-positive progenitor-like microglial population is resistant to CSF1R inhibition in adult mouse brain. Elife *9*. 10.7554/eLife.51796.

998   43.   PubChem (2023). Compound Summary for CID 53481124, Ganglioside GD2 (d18:0/24:1(15Z)). National Center for Biotechnology Information.

1000   44.   Van Oekelen, O., Aleman, A., Upadhyaya, B., Schnakenberg, S., Madduri, D., Gavane, S., Teruya-Feldstein, J., Crary, J.F., Fowkes, M.E., Stacy, C.B., et al. (2021). Neurocognitive and hypokinetic movement disorder with features of parkinsonism after BCMA-targeting CAR-T cell therapy. Nat Med *27*, 2099-2103. 10.1038/s41591-021-01564-7.

1004   45.   Shultz, L.D., Goodwin, N., Ishikawa, F., Hosur, V., Lyons, B.L., and Greiner, D.L. (2014). Human cancer growth and therapy in immunodeficient mouse models. Cold Spring Harb Protoc *2014*, 694-708. 10.1101/pdb.top073585.

1007   46.   Guttenplan, K.A., Weigel, M.K., Prakash, P., Wijewardhane, P.R., Hasel, P., Rufen-Blanchette, U., Münch, A.E., Blum, J.A., Fine, J., Neal, M.C., et al. (2021). Neurotoxic reactive astrocytes induce cell death via saturated lipids. Nature *599*, 102-107. 10.1038/s41586-021-03960-y.

1011   47.   Parihar, V.K., and Limoli, C.L. (2013). Cranial irradiation compromises neuronal architecture in the hippocampus. Proc Natl Acad Sci U S A *110*, 12822-12827. 10.1073/pnas.1307301110.

1014   48.   Andres, A.L., Gong, X., Di, K., and Bota, D.A. (2014). Low-doses of cisplatin injure hippocampal synapses: a mechanism for 'chemo' brain? Exp Neurol *255*, 137-144. 10.1016/j.expneurol.2014.02.020.

1017   49.   Kempf, S.J., Casciati, A., Buratovic, S., Janik, D., von Toerne, C., Ueffing, M., Neff, F., Moertl, S., Stenerlöw, B., Saran, A., et al. (2014). The cognitive defects of neonatally irradiated mice are accompanied by changed synaptic plasticity, adult neurogenesis and neuroinflammation. Mol Neurodegener *9*, 57. 10.1186/1750-1326-9-57.

1021   50.   Jang, A., Petrova, B., Cheong, T.C., Zawadzki, M.E., Jones, J.K., Culhane, A.J., Shipley, F.B., Chiarle, R., Wong, E.T., Kanarek, N., and Lehtinen, M.K. (2022). Choroid plexus-CSF-

1023   targeted antioxidant therapy protects the brain from toxicity of cancer chemotherapy.
1024   Neuron *110*, 3288-3301.e3288. 10.1016/j.neuron.2022.08.009.
1025   51.   Iram, T., Kern, F., Kaur, A., Myneni, S., Morningstar, A.R., Shin, H., Garcia, M.A., Yerra, L.,
1026   Palovics, R., Yang, A.C., et al. (2022). Young CSF restores oligodendrogenesis and memory
1027   in aged mice via Fgf17. Nature *605*, 509-515. 10.1038/s41586-022-04722-0.
1028   52.   Walker, A.J., Majzner, R.G., Zhang, L., Wanhainen, K., Long, A.H., Nguyen, S.M., Lopomo,
1029   P., Vigny, M., Fry, T.J., Orentas, R.J., and Mackall, C.L. (2017). Tumor Antigen and Receptor
1030   Densities Regulate Efficacy of a Chimeric Antigen Receptor Targeting Anaplastic
1031   Lymphoma Kinase. Mol Ther *25*, 2189-2201. 10.1016/j.ymthe.2017.06.008.
1032   53.   Sen, G., Chakraborty, M., Foon, K.A., Reisfeld, R.A., and Bhattacharya-Chatterjee, M.B.
1033   (1998). Induction of IgG antibodies by an anti-idiotype antibody mimicking
1034   disialoganglioside GD2. J Immunother *21*, 75-83. 10.1097/00002371-199801000-00010.
1035   54.   Jena, B., Maiti, S., Huls, H., Singh, H., Lee, D.A., Champlin, R.E., and Cooper, L.J. (2013).
1036   Chimeric antigen receptor (CAR)-specific monoclonal antibody to detect CD19-specific T
1037   cells in clinical trials. PLoS One *8*, e57838. 10.1371/journal.pone.0057838.
1038

1039 **KEY RESOURCES TABLE**

REAGENT or RESOURCE	SOURCE	IDENTIFIER
Antibodies		
Rabbit anti-IBA1	Wako Chemicals	Cat#019-19741; RRID: AB_839504
Rat anti-CD68	Abcam	Cat#ab53444; RRID: AB_869007
Rabbit anti-DCX	Abcam	Cat#ab18723; RRID: AB_732011
Rabbit anti-ASPA	EMD Millipore	Cat#ABN1698; RRID: AB_2827931
Goat anti-PDGFRa	R&D Systems	Cat#AF1062; RRID: AB_2236897
Alexa 647 donkey anti-rabbit IgG	Jackson Immunoresearch	Cat# 711-605-152; RRID: AB_2492288
Alexa 488 donkey anti rat IgG	Jackson Immunoresearch	Cat# 712-545-153; RRID: AB_2340684

Alexa 594 donkey anti-rabbit IgG	Jackson Immunoresearch	Cat# 711-585-152; RRID: AB_2340621
Alexa 488 donkey anti goat IgG	Jackson Immunoresearch	Cat# 705-545-147; RRID: AB_2336933
Alexa 647 donkey anti-mouse IgG	Jackson Immunoresearch	Cat# 715-605-150; RRID: AB_2340862
DAPI	Thermo Fisher Scientific	Cat# 62247;
Prolong Gold Mounting Medium	Life Technologies	Cat# P36930;
Normal Donkey Serum	Jackson Immunotherapy	Cat# 017-000-121
Anti-14G2a idiotype anytibody (clone 1A7)	NCI	
Anti-FMC63 idiotype antibody	MD Anderson Cancer Center	L. Cooper
DyLight 650 Microscale Antibody Labeling Kit	Invitrogen	84536
Bacterial and virus strains		
pCMV6-XL5 vector	Origene	PCMV6XL5
Biological samples		
Chemicals, peptides, and recombinant proteins		
8% Glutaraldehyde	Electron Microscopy Services	Cat#16000
16% Paraformaldehyde	Electron Microscopy Services	Cat#15700
0.1 M sodium cacodylate	Electron Microscopy Services	Cat#12300
Lipofectamine 2000	Life Technologies	11668027
RPMI-1640 Medium	Gibco	11875119
FBS	Gibco	A4736401
HEPES	Gibco	15630080

GlutaMAX	Gibco	35050061
Penicillin- Streptomycin	Gibco	15070063
Ficoll-Paque Plus	GE Healthcare	17-1440
CryoStor CS10 Freeze Media	Sigma Aldrich	C2874
Poly-D-lysine	Corning	354210
DMEM	Gibco	11960-044
Opti-MEM	Gibco	A4124801
Human T-Activator αCD3/CD28 Dynabeads	Gibco	11132D
AIM-V Media	Gibco	12055083
Human IL-2	Peprotech	200-02
RectroNectin	Takara Bio	T100A
Critical commercial assays		
Immune Monitoring 48-Plex Mouse ProcartaPlex™ Panel	Thermo Fisher Scientific	Cat# EPX480-20834-901
Deposited data		
Experimental models: Cell lines		
143B	ATCC	CRL-8303
NALM6	NCI	Gift C. Khanna
MG63.3	UPenn	Gift S. Grupp
293GP		
Experimental models: Organisms/strains		
NOD.Cg-*Prkdc^{scid} Il2rg^{tm1Wjl}*/SzJ	The Jackson Laboratory	Strain #:005557
Oligonucleotides		
Homo sapiens CD19 antigen (CD19), mRNA		NM_001770.3
Recombinant DNA		

Software and algorithms		
FIJI	NIH	https://imagej.net/software/fiji/
Zen	Zeiss	https://www.zeiss.com/microscopy/us/products/microscope-software/zen.html
Imaris image analysis software	Oxford Instruments	https://imaris.oxinst.com/packages
Graphpad Prism	Dotmatics	https://www.graphpad.com/
Other		
FACSAria II	BD Biosciences	
Buffy Coats	Stanford Blood Center	

1040

STAR Methods

RESOURCE AVAILABILITY

Lead Contact: Further information and requests for resources and reagents should be directed to and will be fulfilled by Michelle Monje (mmonje@stanford.edu)

Materials Availability:

Data and Code Availability

EXPERIMENTAL METHOD AND SUBJECT DETAILS

Cell and Culture conditions
The Nalm6-GFP Luciferase B-ALL cell line was obtained from S. Grupp (University of Pennsylvania, Philadelphia, PA). The 143B cell line was obtained from ATCC and was transfected with CD19 (NM_001770.3) in the pCMV6-XL5 vector (Origene) using Lipofectamine 2000 (Life Technologies). Transfected cells have been sorted (FACSAria II, BD Bioscience) and single cell cloned to obtain a pure population [24]. MG63.3 was obtained by C. Khanna (NCI, NIH, Bethesda, MD). All the cell lines were cultured in RPMI-1640 medium (Gibco) supplemented with 10% FBS, 10 mM HEPES, 2 mM GlutaMAX, 100 U/mL penicillin, and 100 µg/mL streptomycin (Gibco).

PBMC isolation

1062 Buffy coats, leukopaks or Leukocyte Reduction System (LRS) chambers from healthy donor were
1063 obtained through the Stanford Blood Center under an IRB-exempt protocol. Peripheral blood
1064 mononuclear cells were isolated using Ficoll-Paque Plus (GE Healthcare, 17-1440) density
1065 gradient centrifugation according to the manufacturer's instructions and cryopreserved with
1066 CryoStor CS10 freeze media (Sigma-Aldrich) in 2-5 x 10^7 cell aliquots.
1067
1068

1069 **CAR construction**
1070 The GD2-4-1-BBz and CD19-4-1-BBz CARs have been previously described [24] and were
1071 generated by cloning the scFvs derived from the 14G2a and FMC63 antibodies into the MSGV1
1072 retroviral vector. In some experiments, CAR vectors including the mcherry reporter gene after the
1073 CD3z signaling domain were used.
1074

1075 **Virus production**
1076 Retroviral supernatant was generated as previously described [24]. Briefly, 6-7 M of 293GP cells
1077 were plated on 100mm poly-D-lysine (Corning) coated plates in complete DMEM media
1078 supplemented with 10% FBS, 10 mM HEPES, 2 mM GlutaMAX, 100 U/mL penicillin, and 100
1079 µg/mL streptomycin (Gibco). The day after, cells were transfected with 4.5 µg of RD114 and 9 µg
1080 of the CAR plasmid using Lipofectamine 2000 (Invitrogen) in Opti-MEM media (Gibco). Media
1081 was changed 24 hours after transfection. The supernatant was harvested after 48 and 72 hours
1082 and stored at -80°C until use.
1083

1084 **CAR T generation**
1085

1086 CAR T cells were generated as previously described [52] (Walker, A. J. et al. Tumor Antigen and
1087 Receptor Densities Regulate Efficacy of a Chimeric Antigen Receptor Targeting Anaplastic
1088 Lymphoma Kinase. Molecular Therapy 25, 2189-2201, doi:10.1016/j.ymthe.2017.06.008). Briefly,
1089 at day 0, PBMCs were thawed and activated with Human T-Activator αCD3/CD28 Dynabeads
1090 (Gibco) at a 3:1 bead to cell ratio, in AIM-V media (Gibco) supplemented with 5% FBS, 10 mM
1091 HEPES, 2 mM GlutaMAX, 100 U/mL penicillin, 100 µg/mL streptomycin, and 100 U/mL
1092 recombinant human IL-2 (Peprotech). Retroviral transduction was done on day 3 and 4 by using
1093 non-tissue culture treated plates previously coated with RetroNectin (Takara Bio) according to
1094 manufacturer's instructions. One mL of retroviral supernatant was added and the plates were then
1095 centrifuged at 3,200 RPM at 32°C for 2 hours. The supernatant was then removed and 0.5 x 106
1096 T cells were added to each well in 1 mL of complete AIM-V media. The Dynabeads were removed
1097 on day 5 by magnetic separation and the T cells were maintained in culture at a density between
1098 0.3 – 0.5x106 cells/mL until Day 10, with media changes every 2-3 days.
1099

1100 **Flow cytometry**
1101

1102 GD2 CAR expression was verified by using the anti-14G2a idiotype antibody (clone 1A7) obtained
1103 from National Cancer Institute[53], together with mCherry detection, when present. CD19 CAR
1104 expression was detected with an anti-FMC63 idiotype antibody provided by L. Cooper (MD
1105 Anderson Cancer Center)[54]. Idiotype antibodies were fluorescently labeled with the DyLight 650
1106 Microscale Antibody Labeling Kit (Invitrogen). The cells were washed and stained in FACS buffer
1107 (PBS supplemented with 2% FBS) for 20 minutes at 4°C. Flow cytometry was performed on a BD
1108 Fortessa instrument.
1109

1110 **Mouse models**
1111

All studies were conducted with NSG mice (NOD-SCID-IL2R gamma chain-deficient, Jackson Laboratories). Males and females were used equally, and all animals were housed at Stanford University; all procedures complied with Institutional Animal Care and Use Committee protocol at Stanford. Animals were housed in a standard 12h light: 12h dark cycle with ad libitum access to food and water.

Diffuse Intrinsic Pontine Glioma *in vivo* model

For the orthotopic xenograft DIPG model, NSG mice were bred at Stanford following all approved protocols. Pups between the ages of P0-P3 were anesthetized by cryoanesthesia. Mice were placed on a piece of sterile gauze on ice until they are no longer moving. Then mice were stabilized on a stereotactic surgical frame (Stoelting) cooled down to ensure continuous deep cryoanesthesia of the pups. A single cell suspension of SU-DIPG-VI-GFP was prepared in sterile HBSS immediately before injection. Approximately 100,000 cells in 2ul of HBSS was injected at a rate of 0.5 microliter per minute using a 33 gauge Hamilton needle into the fourth ventricle of the brain at the following coordinates: 3 mm dorsal to bregma and 3 mm deep to cranial surface. The needle remained in the brain for one minute before retraction and animals were monitored after surgery while they recovered on a heating pad. Mice were then returned to their mother and monitored until normal weaning at P21. Eight weeks after tumor injection, mice are assessed for tumor burden via in vivo luminescence imaging (IVIS Spectrum, Perkin Elmer) and total flux was calculated using the machine's software (Living Image, Perkin Elmer) measured as circular ROIs centered over the mouse's skull. Mice were ranked by tumor burden and then sequentially distributed over three different groups: GD2-4-1-BBz CAR T-cells (therapeutic), CD19-4-1-BBz CAR T-cells (non-targeting controls), or mock T-cells (activated but not infected with a viral construct). Mice were administered $1x10^7$ transduced cells in 200 microliters sterile HBSS. Tumor burden was measured weekly by IVIS to determine successful tumor clearance. Tumors were clear by D21 post injection, and then animals were left undisturbed in their home cages for two weeks after tumor clearance. On D35 post CAR T-cell injection, animals were subjected to behavioral assays and then CSF and brains were collected as described below.

Acute Lymphoblastic Leukemia *in vivo* model

Nalm6-GFP Luciferase B-ALL cells were cultured and expanded as described above and harvested with TrypLE Express (Gibco 12604-013). For the orthotopic model, $1x10^6$ cells in 200ul of sterile HBSS were injected intravenously in male and female mice aged 5-6 weeks. Three days after tumor injection, mice were assessed for tumor burden via IVIS, ranked by tumor burden and sequentially distributed over three groups: CD19-4BBz CAR T-cells (therapeutic), GD2-4BBz CAR T-cells (non-targeting controls), or mock T-cells (activated but not infected with a viral construct). Mice were administered $5x10^6$ transduced cells in 200ul of sterile HBSS and monitored twice a week by IVIS. To avoid infiltration of NALM6 cells to the brain, mock treated animals were assayed for cognitive differences and CSF and brain collection at D10 post NALM6 introduction, and brains were checked histologically for GFP+ cells. CAR T-cell treated animals cleared their tumors by D14 post CAR injection, and then were left undisturbed in their cages until D28, when they were assayed for cognition and tissue collection as described below.

Osteosarcoma *in vivo* models
MG63.3 and 143B-CD19 osteosarcoma lines were cultured and expanded as described above and harvested with TrypLE Express. For the orthotopic model, $1x10^6$ MG63.3 cells or $1x10^6$ 143B-CD19 cells were injected periosteal to the tibia of male and female mice aged 5-7 weeks. In the MG63.3 model, 4 weeks after tumor initiation animals were administered $5x10^6$ transduced GD2-

1163   4BBz CAR T-cells (therapeutic), B7H3 CAR T-cells (therapeutic) or mock T-cells. In the 143B-
1164   CD19 model, 1 week after tumor initiation animals were administered 10×10^6 CD19-4BBz CAR
1165   T-cells (therapeutic) or mock T-cells. Tumors were measured with a digital caliper once a week.
1166   Two weeks after tumor clearance in each model (7D post treatment in MG63.3, 21D post
1167   treatment in 143B-CD19), animals were assayed for cognition and tissue collected as described
1168   below.
1169
1170   **Anakinra treatment in the ALL model**
1171
1172   Mice were engrafted with Nalm6-GFP Luciferase B-ALL cells as described above. Three days
1173   after tumor injection, mice were assessed for tumor burden via IVIS, ranked by tumor burden and
1174   sequentially distributed over four groups: CD19-4BBz CAR T-cells (therapeutic) +/- Anakinra, or
1175   mock T-cells +/- Anakinra. Mice were administered 5×10^6 transduced cells in 200ul of sterile
1176   HBSS and monitored twice a week by IVIS. Beginning on Day 0 of CAR T cell treatment, animals
1177   were administered 10mg/kg of Kineret (Anakinra, Stanford Pharmacy) daily i.p., until Day 14 post
1178   treatment, the duration of tumor clearance. Mock treated animals were again measured for
1179   cognition at D10 post NALM6 engraftment, and CAR T-cell treated animals were left undisturbed
1180   in their cages until D28, when they were assayed for cognition and tissue collection as described
1181   below.
1182
1183
1184   **Microglia Depletion *in vivo* with PLX5622**
1185   To deplete microglia in the brain, mice in both the DIPG and ALL in vivo models were given *ad*
1186   *libitum* access to rodent chow containing 1200ppm of PLX5622 beginning after their tumors
1187   cleared (D21 post treatment in the DIPG model and D14 post treatment in the ALL model) and
1188   maintained on PLX5622 for two weeks. Animals underwent cognitive assays and CSF and brain
1189   collection as described below. PLX5622 was purchased from MedChemExpress (HY-114153)
1190   and formulated in AIN-76A standard chow by Research Diets Inc (D19101002i).
1191
1192   **METHOD DETAILS**
1193
1194   **CSF collection and perfusion**
1195   At the endpoint of each experiment as described above, mice were anesthetized with isoflurane
1196   and mounted onto a stereotactic surgical rig (Stoelting) with the head secured at a 30-degree
1197   angle facing upward. The hair of the neck was shaved and an incision was made through the skin
1198   and muscle. The muscle around the neck was separated with blunt metal forceps to reveal the
1199   cisterna magna. Any extra blood was cleaned with cotton tips until the area was cleared. CSF
1200   was removed from the cisterna magna using a pulled clear capillary glass tube (Harvard
1201   Apparatus 30-0062, 1.5 OD x 1.17 ID x 100mm). CSF was stored in a low binding microcentrifuge
1202   tube (Costar, 3206), then frozen on dry ice and stored at -80 degrees until assayed. After CSF
1203   collection, mice were transcardially perfused with 20ml 0.1M PBS. Brains were fixed in 4% PFA
1204   overnight at $4^{o}C$, before being transferred to 30% sucrose for cryoprotection. Brains were
1205   embedded in Tissue-Tek (Sakura) and sectioned coronally at 40µm using a sliding microtome
1206   (Microm HM450; Thermo Scientific).
1207
1208   **Immunohistochemistry**
1209   For immunohistochemistry, a 1 in 6 series of 40µm coronal sections was incubated in 3% normal
1210   donkey serum in 0.3% Triton X-100 in TBS blocking solution at room temperature for one hour.
1211   Rabbit anti-IBA1 (1:1000, Wako Chemicals 019-19741), rat anti-CD68 (1:200, Abcam ab53444),
1212   rabbit anti-DCX (1:500, Abcam ab18723), rabbit anti-ASPA (1:250, EMD Millipore ABN1698), and
1213   goat anti-PDGFRa (1:500; R&D Systems AF1062) were diluted in 1% normal donkey serum in

1214 0.3% Triton X-100 in TBS and incubated overnight at 4°C. Sections were then rinsed three times
1215 in 1X TBS and incubated in secondary antibody solution (Alexa 647 donkey anti-rabbit IgG, 1:500
1216 (Jackson Immunoresearch); Alexa 488 donkey anti rat IgG, 1:500 (Jackson Immunoresearch);
1217 Alexa 594 donkey anti-rabbit IgG, 1:500 (Jackson Immunoresearch); Alexa 488 donkey anti goat
1218 IgG, 1:500 (Jackson Immunoresearch); Alexa 647 donkey anti-mouse IgG, 1:500 (Jackson
1219 Immunoresearch) in 1% blocking solution at room temperature protected from light for two hours.
1220 Sections were rinsed 3 times in TBS, incubated with DAPI for 5 minutes (1:1000; Thermo Fisher
1221 Scientific) and mounted with ProLong Gold mounting medium (Life Technologies).
1222

1223 **Confocal imaging and quantification**
1224 All cell counting was performed by experimenters blinded to experimental conditions on a Zeiss
1225 LSM700 or LSM980 scanning confocal microscope (Zeiss). Images were taken at 20X
1226 magnification and analyzed using either FIJI software or Imaris software. For microglia imaging,
1227 three consecutive sections ranging approximately from bregma +1.2 to +0.8 were selected for
1228 cortex and corpus callosum, and four consecutive sections ranging approximately from bregma -
1229 1.8 to -2.4 were selected for the hilus of the dentate gyrus. For each section, the superficial cortex,
1230 deep cortex, cingulum, genu of the corpus callosum, and hilus of the dentate gyrus were identified,
1231 and two 219.5 x 219.5 μm fields per slice were selected in those areas for quantification. All CD68^{+}
1232 and IBA1^{+} cells were counted in those regions. For analysis of immature neurons, four
1233 consecutive sections ranging approximately from bregma -1.8 to -2.4 were selected for the
1234 dentate gyrus, and four 219.5 x 219.5 μm fields per slice were selected in those areas for
1235 quantification. All DCX^{+} cells within the inner layer of the dentate gyrus were counted in those
1236 regions. For analysis of oligodendrocytes (ASPA[+]) and oligodendrocyte precursor cells
1237 (PDGFRa[+]) three consecutive sections ranging from bregma +1.2 to +0.8 were stained. The
1238 cingulum and genu of the corpus callosum in each hemisphere was imaged with two 319.5 x
1239 319.5 μm field and cells were quantified using the "Spots" function in Imaris image analysis
1240 software (Oxford Instruments). Each image was manually inspected to ensure accurate
1241 oligodendrocyte counts. False positive and false negative counts were manually removed or
1242 added, respectively.
1243

1244 **Electron Microscopy**
1245 At D35 post CAR T-cell treatment in the DIPG xenograft model, mice were anesthetized with
1246 isoflurane and CSF was collected as described above. Mice were then sacrificed by transcardial
1247 perfusion with Karnovsky's fixative: 2% glutaraldehyde (Electron Microscopy Sciences (EMS
1248 16000) and 4% paraformaldehyde (EMS 15700) in 0.1 M sodium cacodylate (EMS 12300), pH 7.
1249 Samples were prepared as detailed previously in[11]. Axons in the cingulum of the corpus callosum
1250 were analyzed for myelinated axon density (total number of myelinated axons in each frame) by
1251 experimenters who were blinded to experimental conditions and genotypes. A minimum of 500
1252 axons were scored per group.
1253

1254 **Mouse CSF and serum cytokine analysis**
1255 The Luminex multiplex assay was performed by the Human Immune Monitoring Center at
1256 Stanford University. Mouse 48-plex Procarta kits were purchased from Thermo Fisher, Santa
1257 Clara, California, USA, and used according to the manufacturer's recommendations with
1258 modifications as described below. Briefly: beads were added to a 96-well plate and washed in a
1259 Biotek Elx405 washer. Samples were added to the plate containing the mixed antibody-linked
1260 beads and incubated overnight at 4°C with shaking. Cold (4°C) and room temperature incubation
1261 steps were performed on an orbital shaker at 500-600 RPM. Following the overnight incubation
1262 plates were washed in a Biotek Elx405 washer and then biotinylated detection antibody added for
1263 60 minutes at room temperature with shaking. Plate was washed as described above and
1264 streptavidin-PE was added. After incubation for 30 minutes at room temperature, washing was

1265 performed as above and reading buffer was added to the wells. CSF samples were measured as
1266 singlets, while serum samples were measured in duplicate. Plates were read on a FM3D FlexMap
1267 instrument with a lower bound of 50 beads per sample per cytokine. Custom Assay Chex control
1268 beads were purchased from Radix Biosolutions, Georgetown, Texas, and were added to all wells.
1269

1270 **Novel Object Recognition Task**
1271 Cognition was analyzed using a modified version of the novel object recognition task (NORT) that
1272 focused on the attentional component of the task. The test was modified so that the duration
1273 between the training and testing phase was shortened, to ensure that the test placed a greater
1274 cognitive load on short-term (< 5 min) memory, attention, and frontal lobe function rather than
1275 longer-term memory and hippocampal function. In DIPG, aggressive osteosarcoma and rapidly
1276 clearing osteosarcoma models, mice were tested via NORT on D34 post CAR-T cell
1277 administration. In the ALL model, mice were tested on D27 post CAR-T cell administration.
1278

1279 Animals were handled for 3 days leading up to the test for 2 min. After handling, the mice were
1280 then placed in the experimental chamber on D33 for the DIPG, aggressive osteosarcoma and
1281 rapidly clearing osteosarcoma models or D26 for ALL model to acclimatize for 20 min prior to
1282 testing on D34 or P27, respectively. The set up consisted of an opaque Plexiglas experimental
1283 chamber 50cm x 50cm x 50cm, and a camera mounted 115 cm above the chamber. The test was
1284 conducted during the animal's rest phase, in a dark room illuminated with only red light.
1285

1286 On the day of testing, mice were brought to the testing room and allowed to settle in their cages
1287 for 20 minutes prior to any handling. Afterwards, mice were handled for 2 min and then placed in
1288 the chamber to acclimate for 20 min before being returned to the home cage for another 5 min.
1289 Mice were then placed in the experimental chamber with two identical Lego objects (each
1290 approximately 4 cm in size). Each time the mouse was placed into the chamber it was facing the
1291 opaque wall, with the animal's tail in the direction of the objects. For the training phase, the mouse
1292 was allowed to explore the two identical objects for 5 min and then the mouse was returned to
1293 the home cage for 5 min while the experimental chamber and objects were cleaned with 1%
1294 Virkon S broad spectrum disinfectant. During this time, one cleaned object from the sample phase
1295 was placed back into the experimental chamber along with a new Lego object (of similar size) for
1296 the novel object phase. For the novel object testing phase, the mouse was returned to the
1297 experimental chamber and allowed to explore for 10 min.
1298

1299 The objects used as novel and familiar were counterbalanced, as was the position of the novel
1300 object from trial to trial, animal to animal. All of the Lego objects used in the behavioral paradigm
1301 were piloted to ensure that there was no bias, or object preference for the animals. The camera
1302 footage was then analyzed using Noldus analysis software and any exploratory head gesturing
1303 within 2 cm of the Lego object, including sniffing and biting, was considered object investigation,
1304 but sitting on the object, or casual touching of the object in passing was not considered object
1305 investigation (Leger et al., 2013). Only animals that explored both of the identical objects during
1306 the testing phase for an accumulation of a minimum of 20 s were included in the analysis. The
1307 Recognition Ratio was determined by taking the ratio of the amount of time spent investigating
1308 one object compared to the total time spent investigating both objects (i.e., time spent with Novel
1309 Object / (time spent with Novel Object + time spent with Familiar Object)).
1310

1311 **Spontaneous Alternation T Maze Task**
1312 Hippocampal-dependent cognitive performance was analyzed using the spontaneous alternation
1313 T maze task, which focuses on assessing spatial working memory. This test was administered
1314 over 2 days beginning at the end of the NORT assessment. DIPG, aggressive osteosarcoma and
1315 rapidly clearing osteosarcoma models were tested on D34 and D35 post CAR-T cell

1316 administration. The ALL model was tested on D27 and D28 post CAR-T cell administration. At
1317 this point, mice had been handled prior to, and during NORT. The test was conducted during the
1318 animal's rest phase, in a dark room illuminated with only red light. The T maze set up consisted
1319 of a start arm and two goal arms, each 30 X 10 cm with 20 cm high walls, where one goal arm of
1320 the T maze is textured to allow for clear distinction by the mouse[28].

1322 For day 1 of the T maze assessment, after NORT had been completed and mice given at least 2
1323 hours of rest, a mouse is placed at the base of a T-shaped maze facing away from the goal arms.
1324 As the mouse explores the maze, it chooses an arm. After arm selection, by virtue of having four
1325 paws in that arm, a guillotine door was closed to allow the mouse to only explore and familiarize
1326 itself with the chosen arm for 30 s. The mouse was then placed back at the base of the maze
1327 facing away from the goal arms. This process was repeated for 11 consecutive cycles allowing
1328 for 10 total choices.

1330 On day 2, mice were brought into the testing room and allowed to settle in their cages for 20
1331 minutes prior to any handling. Afterwards, mice are each handled for 2 minutes prior to T maze
1332 testing. Next, a mouse was placed at the base of a T-shaped maze facing away from the goal
1333 arms. The mouse then chose an arm by having four paws in that arm. At that moment, the
1334 guillotine door was closed to allow the mouse to explore the chosen arm for 30 s. The mouse was
1335 then returned to its home cage for 15 min. The mouse was then placed back at the base of the
1336 maze facing away from the goal arms and allowed to explore and choose a goal arm. This process
1337 was repeated for 11 consecutive cycles. The chosen arms were recorded during testing and mice
1338 were scored over 10 trials.

1340 **QUANTIFICATION AND STATISTICAL ANALYSIS**

1342 For all quantifications, experimenters were blinded to sample identity and condition.

1344 For fluorescent immunohistochemistry and confocal microscopy, images were taken at 20X and
1345 cells considered co-labeled when markers co-localized within the same plane. For cortical/white
1346 matter microglia staining three sections per mouse, eight frames in standardized locations per
1347 section (24 images per mouse) were counted, for hippocampal microglia staining, four sections
1348 per mouse, 2 frames in standardized location per section (8 images per mouse) were counted.
1349 For hippocampal neuroblast staining, four sections per mouse, 4 frames in standardized location
1350 per section (16 images per mouse) were counted. For oligodendrocyte staining three sections per
1351 mouse, 8 frames in standardized location per section (24 images per mouse) were counted. For
1352 each mouse, 300-700 cells were counted for each immunohistochemical marker analysis. The
1353 density of cells was determined by dividing the total number of cells quantified for each lineage
1354 by the total volume of the imaged frames (mm^3). In all experiments, "n" refers to the number of
1355 mice. In every experiment, "n" equals at least 3 mice per group; the exact "n" for each experiment
1356 is defined in the figure legends.

1358 For electron microscopy (EM) quantification of myelinated axon density, 6000X images were
1359 obtained. For myelinated axon density, the number of axons surrounded by a myelin sheath were
1360 counted and normalized to tissue area. 29 images were scored for each mouse. Approximately
1361 400-700 axons were scored for each mouse.

1364 All statistics were performed using Prism Software (Graphpad). For all analyses involving
1365 comparisons of one or two variables, 1-way or 2-way ANOVAs, respectively, were used with
1366 Tukey's multiple comparisons post hoc corrections used to assess main group differences. For

1367   analyses involving only two groups, unpaired two-tailed Student's t tests were used. For
1368   measurements of individual cytokine levels, unpaired two-tailed Student's t tests were used
1369   without correction for multiple comparisons. Shapiro-Wilk test was used to determine normality
1370   for all datasets; all datasets were parametric. A level of $p < 0.05$ was used to designate significant
1371   differences.
1372
1373
1374
1375